A robust wavelet-based approach for dominant frequency analysis of atrial fibrillation in body surface signals

V. G. Marques[1], M. Rodrigo[2], M. S. Guillem[2], J. Salinet[1]

[1] Biomedical Engineering, Center for Engineering, Modeling and Applied Social Sciences, Federal University of ABC, Brazil

[2] ITACA Institute, Universitat Politècnica de València, Spain

Corresponding author:

João Salinet

Biomedical Engineering

Center for Engineering, Modeling and Applied Social Sciences (CECS)

Federal University of ABC, São Bernardo do Campo, São Paulo, Brazil

Address: Alameda da Universidade, s/n - Anchieta 09606-045

Email: joao.salinet@ufabc.edu.br

Phone: +55 11 2320 – 6342

ORCID: 0000-0003-2906-9397

Abstract

Objective: Atrial dominant frequency (DF) maps undergoing atrial fibrillation (AF) presented good spatial correlation with those obtained with the non-invasive body surface potential mapping (BSPM). In this study, a robust BSPM-DF calculation method based on wavelet analysis is proposed.

Approach: Continuous wavelet transform along 40 scales in the pseudo-frequency range of 3-30 Hz is performed in each BSPM signal using a Gaussian mother wavelet. DFs are estimated from the intervals between the peaks, representing the activation times, in the maximum energy scale. The results are compared with the traditionally widely applied Welch periodogram and the robustness was tested on different protocols: increasing levels of white Gaussian noise, artificial DF harmonics presence and reduction of number of leads. 11 AF simulations and 12 AF patients are considered in the analysis. For each patient, intracardiac electrograms were acquired in 15 locations from both atria. The accuracy of both methods was assessed by calculating the absolute errors of the HDF_{BSPM} with respect to the atrial HDF, either simulated or intracardially measured, and assumed correct if ≤ 1 Hz. The spatial distribution of the errors between torso DFs and atrial HDFs were compared with atria driving mechanisms location. Torso HDF regions, defined as portions of the maps with $|DF - \text{HDF}_{BSPM}| \leq 0.5$ Hz were identified and the percentage of the torso occupied these regions was compared between methods.

Main results: The proposed method allowed a significant improvement on non-invasive estimation of the atria HDF (median relative error of 7.14% vs. 60.00%, p = 0.06), outperforming the Welch approach in correct estimations of atrial HDFs non-invasively for both cases: models (81.82% vs 45.45%) and patients (75.00% vs 66.67%). A low positive BSPM-DF maps correlation was seen between techniques (0.47 for models and 0.63 for patients), highlighting overall differences in DF distributions. The method was more robust to white Gaussian noise and harmonics and presented more consistent results in lead layouts with low spatial resolution ($p = 0.99$ vs. $p = 0.94$).

Significance: Estimation of atrial HDFs using BSPM is improved by the proposed wavelet-based algorithm, helping increase the non-invasive diagnostic ability in AF.

Keywords: atrial fibrillation, non-invasive, dominant frequency, wavelet, body surface potential mapping

1 Introduction

Atrial fibrillation (AF) is the most common cardiac arrhythmia in clinical practice, with an estimated prevalence of 3% in the population above 20 years, a percentage that tends to increase with the aging population [1]. AF is associated with high mortality and morbidity, mainly due to an increased risk of thromboembolic events such as strokes [1]. The mechanisms behind AF are complex and not yet completely understood [1]. Recent studies have related the maintenance of AF to localized regions, which can then be targeted for ablation, improving the therapy outcomes by following personalized approaches [2], [3]

Invasive electrophysiological studies, in which cardiac electrograms (EGMs) are measured directly in the atria using mapping catheters, are the most straightforward approach to identifying regions maintaining AF. However, this strategy is technically complex, demanding a large amount of time, resources and with risks for the patients, motivating the development of non-invasive methods [4]–[7], such as body surface potential mapping (BSPM) and electrocardiographic imaging (ECGi) [4]. Both these techniques are based on the measurement of electrocardiograms, which are then used to obtain information about the atrial behavior, either by directly analyzing the signals [4] or, with the aid of an imaging technique, by using inverse problem analysis and estimating epicardial (or endocardial) electrical activity [8]. Among these techniques, BSPM is the simplest approach, demanding relatively simple hardware and software to analyze the signals, and yielding relevant clinical results [6], [7], [9], which can be of use both in early diagnosis and follow-up [7], [10].

AF was traditionally thought to be maintained by disorganized conduction in the atria, with multiple wavelets that coexist and present no discernible pattern [11]. This view has been challenged by experiments both in animal models and patients, where spatiotemporally organized activity has been identified in the form of high-frequency sources (rotors and/or focal activity), which are thought to maintain the fibrillatory conduction [11], [12]. Locating these AF drivers relies on the identification of regions with a fast activation rate, but this is often a challenging task using time analysis of the complex AF EGMs [13]. Thus, researchers have migrated to analysis in the frequency domain in an attempt to overcome this barrier.

Researchers using spectral analysis have shown that AF signals have important periodic elements with varying degrees of regularity. It has also been shown that signals from certain regions

of the atria may have higher frequency components than those from other regions, suggesting that these areas may be the drivers that maintain AF and could be targets for ablation [11], [13]. It was noticed that the duration of the AF cycle in the left atrium (LA) correlates with the highest power peak of the related spectrum, defined as the dominant frequency (DF) [11]. DF analysis allowed to identify micro-reentries, discrete sites of periodic high-frequency activity responsible for AF maintenance [11], improving the current knowledge of this complex arrhythmia.

DF analysis of EGMs has led to the development of new ablation strategies that target high frequency regions in the atria [12], [14], [15]. Investigators using this approach achieved rates of success as high as 88% and 56% in paroxysmal and persistent AF, respectively [14], and managed to reduce the frequency gradient between the left and right atria, related to the maintenance and recurrence of the arrhythmia [14]. Recently, investigators showed that the highest DF (HDF) areas responsible for AF maintenance can be identified non-invasively through the BSPM DF mapping [9], even with the low-pass filter effect intrinsically related to the volume conductor effect present within the heart and torso [10], providing a valuable clinical tool which can be used prior invasive mapping. Therefore, it is important for new studies to check whether the clinically useful parameter (atrial HDF) can also be precisely detected on the torso. Moreover, since there is no gold standard methodology for non-invasive DF estimation, researchers made use of the widely applied approach based on peak detection in Welch periodograms.

Nonetheless, Fourier based DF analysis presents important limitations, such as the lack of the identification of specific activation times and sensitivity to signal uncertainties such as the presence of harmonic activity and dynamic changes in frequency and phase [13], [16]. Although parallel observation of time signals can mitigate some of these issues [13], a more robust solution is desirable for automatic applications.

A possible alternative for traditional Fourier based DF analysis is using wavelet transform, which can be understood as a generalization of the Fourier transform in which the sine waves are replaced by stretched, squeezed and translated versions of a single waveform, called mother wavelet [17]. The signal is then decomposed in scales rather than frequencies, which are related to a bandwidth, depending on the chosen wavelet. Wavelet transform is a technique with good localization in both time and frequency domains and has the ability to identify points with close to singular behavior [18], such as the sharp transitions associated with activations in BSPM. Pre-

vious studies have used wavelet transforms in the analysis of AF signals, but have been focused in reconstructed epicardial signals rather than in BSPM [19] or have performed analyses based on the energy of scales rather than identified activations [17].

In this study, we proposed a wavelet-based method for estimating atrial HDFs based on the identification of individual activation times. This technique outperformed the Welch periodogram for estimating non-invasively the frequency activity of the AF mechanism, even under noisy conditions, harmonic activity and relative low number of leads in the BSPM layout.

2 Methods

2.1 AF models

A realistic 3D model of the atrial anatomy composed by 284,578 nodes and 1,353,783 tetrahedrons ($673.4 \pm 130.3 \mu m$ between nodes)[20], [21] was used to simulate the atrial electrical activity. A gradient on the electrophysiological properties of the atrial myocardium, specifically on I_{K1}, I_{Na} and I_{CaL} [22], was introduced into the atrial cell formulation [22] to obtain AF propagation patterns maintained by rotors and with spatial variations in the activation rate. Fibrotic tissue was modeled by electrically disconnecting a spatial random amount between 20% and 60% of the total nodes in order to create AF patterns with dominant regions with different shape and extension. The system of differential equations in the atrial cell model was solved by using Runge-Kutta integration based on a graphic processors unit (NVIDIA Tesla C2075 6G) [23]. The stimulation protocol for rotor formation consisted in a S1S2 protocol, with a plane S1 wave and a square S2 wave.

An ensemble of 11 rotor driven AF simulations with 4 seconds each and localized in different portions of the LA and right atrium (RA) were used for the analyses [24]. An uniform mesh (2048 points, 0.51 ± 0.26 cm between nodes) of unipolar EGMs obtained with the models were preprocessed as described elsewhere [24] and DF values were determined in each of the EGMs by detecting the highest power peak in Welch periodograms (80% overlap, zero-padded to achieve a spectral resolution of 0.01 Hz)[9], [24]. DF values were manually inspected and compared with the activation counts to avoid inconsistent detections. The atrial HDF at the location of the functional rotor was defined as the driving frequency of AF. Table 1 summarizes the details of the simulations.

Table 1: Characteristics of the simulations

Model	Rotor location	Atrial HDF (Hz)
1	LA	4.80
2	LA	5.60
3	Left inferior pulmonary vein (LA)	5.50
4	Left superior pulmonary vein (LA)	7.80
5	RA	7.60
6	RA	5.40
7	RA appendage	5.80
8	RA appendage	5.80
9	Right inferior pulmonary vein (LA)	5.50
10	Right inferior pulmonary vein (LA)	5.40
11	Right superior pulmonary vein (LA)	6.80

LA: left atrium; RA: right atrium

BSPM signals were obtained by solving the forward problem with the boundary element method, resulting in 771 nodes with signals referenced to the Wilson central terminal and sampled at f_S = 500 Hz [24], of which 567 points were selected to represent leads of a realistic measurement, excluding points inside the waist, neck or arms. White Gaussian noise was added to the BSPM signals with a signal-to-noise ratio (SNR) of 60 dB[24].

2.2 Patient data

67 BSPM leads were recorded on the torso from 12 patients admitted for ablation of drug-refractory paroxysmal and persistent AF (Table 2) [9]. Simultaneously, intracardiac EGMs were acquired in 15 locations from both atria (f_S = 977 Hz) [9]: the following catheters were introduced via the right femoral vein: (1) a standard tetrapolar catheter in the RA appendage; (2) a deflectable 4-mm mapping catheter (Marinr; Medtronic Inc., Minneapolis, MN) in the distal coronary sinus; (3) a decapolar circular mapping Lasso catheter (Biosense-Webster, Diamond Bar, CA) used to map the pulmonary veins LA junctions; and (4) a Navistar catheter (3.5-mm tip, 2-5-2 interelectrode

distance; Thermo-Cool, Biosense-Webster, Diamond Bar, CA). Bipolar atrial EGMs were recorded by using the CARTO navigation system with embedded spectral analysis capabilities (CARTO XP, version 7.7; Biosense-Webster, Diamond Bar, CA). Signals were then band-pass filtered (40 - 250 Hz), rectified, and then low-pass filtered (20 Hz).

4-second segments within the longest RR interval after the administration of adenosine were used for the analysis of atrial EGMs and BSPM. In 3 patients, QRS complexes were canceled, as the RR intervals were shorter than 4 seconds. DFs in atrial EGMs were determined in each location by detecting the peak with the highest frequency power in Welch periodograms [11]. To avoid inconsistencies, the local activations were detected and manually inspected simultaneously to the DF estimation of atrial signals by Welch, allowing the frequency of activations to be obtained. The atrial HDF was determined and its location was defined as the main driving region of the arrhythmia in the patients (Table 2).

Table 2: Characteristics of the patients

Patient	Age	Gender	AF type	Atrial HDF (Hz)	HDF location
1	47	M	Paroxysmal	10.75	RA
2	54	M	Paroxysmal	10.25	LA
3	64	M	Paroxysmal	13.25	RA
4	49	M	Paroxysmal	9.75	RA
5	51	M	Paroxysmal	10.00	RA
6	60	M	Persistent	10.00	RA
7	61	M	Paroxysmal	9.25	RA
8	47	M	Persistent	9.25	RA
9	59	M	Persistent	6.50	LA
10	68	F	Paroxysmal	11.50	RA
11	67	M	Paroxysmal	6.00	RA
12	47	M	Paroxysmal	7.00	LA

F: female; M: male; LA: left atrium; RA: right atrium

2.3 Preprocessing of BSPM signals

The three-dimensional coordinates of the BSPM nodes in the models were mapped to a two-dimensional configuration by projecting their positions into a cylinder wall. This cylinder has the same height as the torso (61.5 cm) and is centered at the barycenter of the coordinates from all BSPM nodes; the radius is the largest horizontal distance between any point and the center of the cylinder (22.5 cm). The cylinder was unwrapped to a rectangle with the left side of the torso at the center. Electrode positions in patients were arranged in a two-dimensional configuration based on the lead layout (Supplementary Fig. 1); distances between adjacent electrode columns and rows were set at 5 cm. The signals from both models and patients were interpolated into a 30 X 65 grid using cubic splines.

Filtering was performed, when indicated in the methodology, as following: the baseline was estimated by downsampling the signal to $0.025 \cdot f_S$ Hz and low-pass filtering at 0.5 Hz (10th order Butterworth). Baseline signals were then interpolated to their initial f_S and subtracted from the original signals [5]. A low-pass filter (10th order Butterworth) was applied at 30 Hz, covering the spectral range of AF [5].

2.4 DF detection on surface signals

DFs were estimated using a method based on continuous wavelet transform (CWT) modulus maxima detection [19]. When CWT is performed using a wavelet that is the derivative of a smooth function, the extreme points on the results correspond to sharp deflections on the original signal, similar to singularities [18]. This characteristic can be used to detect sharp deflections on BSPM, associated with depolarization wavefronts [25].

Thus, for each lead, CWT was applied on the unfiltered signals using a negative first-order Gaussian mother wavelet (Eq. 1, where C is a normalization constant so that the L2-norm of ψ is equal to 1) along 40 linearly spaced scales in the pseudo-frequency range of 3 to 30 Hz. In order to detect the most physiologically relevant positive deflections, the scale with the highest energy was selected for further processing (Eq. 2, where n are indexes, a are scales and W_a is the CWT of the signal at that scale); the rationale is that this scale contains the most information about a signal and thus represents better its main properties, such as the activation patterns in a BSPM signal.

A 30 Hz low-pass filter (4th order Butterworth) was applied to the scale with the maximum en-

ergy to avoid high frequency oscillations unrelated to the arrhythmia that may appear after CWT; all local maxima, defined as points with higher amplitude than both of their immediate neighbors, were then detected. The average of the cycle lengths (CL) was determined from the intervals between the detected peaks and used for the DF calculation ($DF = 1/CL$). Fig. 1A gives a schematic overview of the proposed method. Figs. 1B and C depict the signal morphologies and the respective frequency spectra for a 6 Hz sine wave contaminated with white Gaussian noise with SNR of 1 dB, a 6 Hz sinusoidal wave with presence of the first harmonic (12 Hz) with SNR of 1 dB and a typical AF signal collected at anterior portion of the torso of Patient 1.

$$\psi(t) = -C \cdot \frac{de^{-t^2}}{dt} \tag{1}$$

$$E_{max} = \max_{a} \sum_{n} |W_a(n)^2| \tag{2}$$

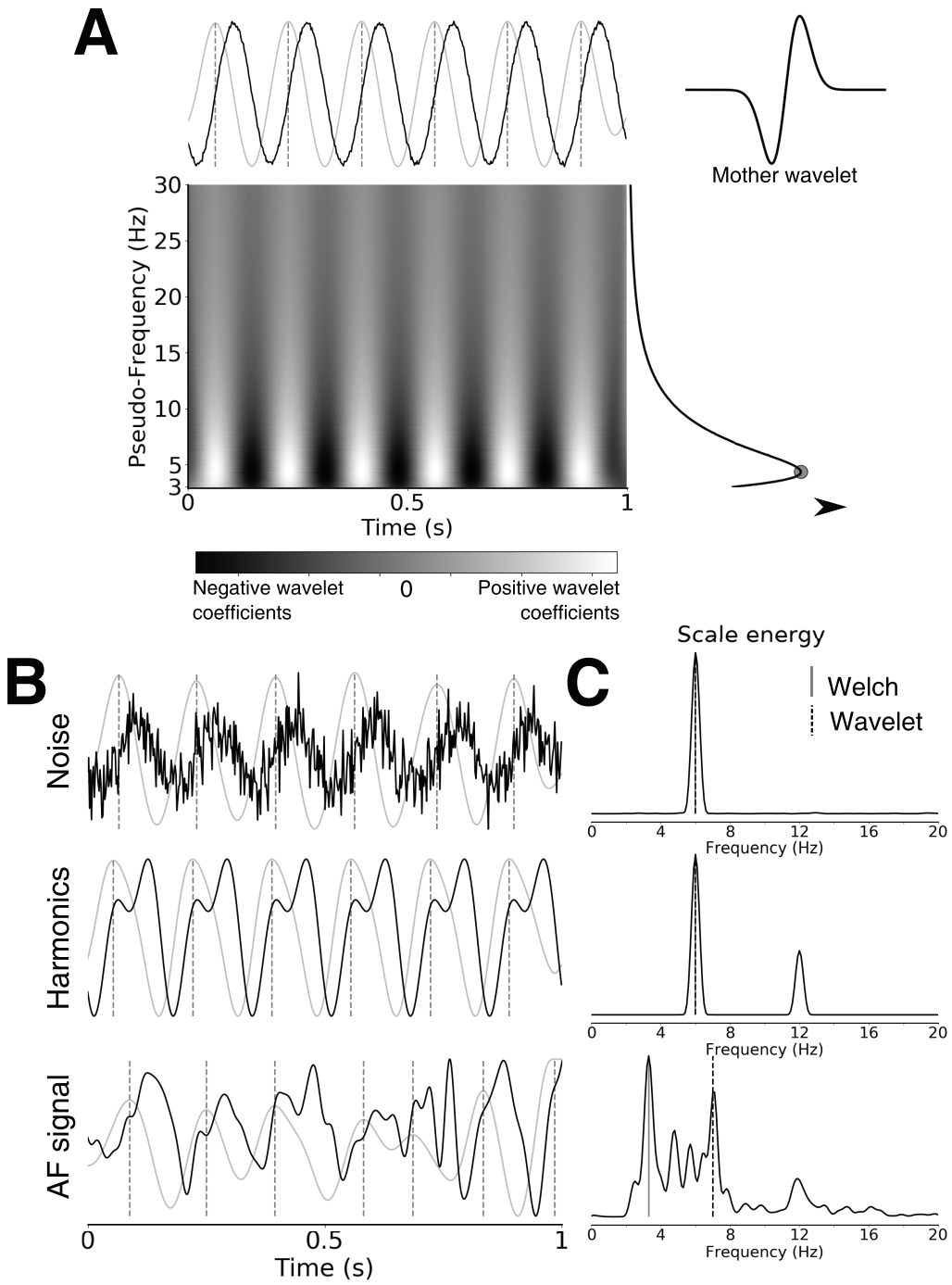

Figure 1: Wavelet method for activation detection and DF estimation. **A:** Schematic of the method. A signal (sine wave with a frequency of 6 Hz, depicted as a black line on the top plot) is used for CWT analysis using a negative first-order Gaussian mother wavelet. The scalogram (bottom) is generated in the pseudo-frequency range of 3 to 30 Hz and the corresponding energy of each scale is calculated. The scale with the maximum energy (top, gray line) is used for the detection of activations, which correspond to the peaks in this scale (top, dashed lines). The average cycle length is used for DF estimation. **B:** Examples of the application of the method in 1-second segments of different signals. Top: 6 Hz sine wave with white Gaussian noise at a SNR of 1 dB. Middle: 6 Hz sinusoidal wave with the presence of a harmonic noise (12 Hz) with SNR of 1 dB. Bottom: signal from the anterior portion of the torso of Patient 1. Black lines represent the original signal, while the gray lines are the CWT at the scale of maximum energy. Dotted lines mark the peaks in the CWT, corresponding to sharp deflections in the original signal. **C:** Corresponding Welch periodograms of the signals in B; the solid line marks the periodogram's highest peak, while the dashed line marks the wavelet estimate. It is possible to see that the method is robust to noise and harmonics in simulated signals, detecting only the inflections related to the signal itself. In the AF signal, only the main repetitive pattern is detected; in this case, the highest peak in the Welch periodogram does not correspond to the DF estimated by the wavelet method.

DFs were estimated by both the proposed method and Welch periodogram. The latter was computed using 2.7 s segments with zero-padding to achieve a frequency step of 0.1 Hz (i.e. $10 \cdot f_S$ samples), Hanning windows and overlap of 90%. Torso DFs were determined by identifying the peak with the highest power in the periodograms withing the AF physiological frequency range (2-15 Hz) [26].

2.5 Driver frequency estimation and spatial distribution

DF maps were generated for both methods by displaying the color coded DF values in the corresponding positions on torso. Atrial HDF values were estimated using the HDF in the BSPM DF maps (HDF_{BSPM}). The accuracy of both methods was assessed by calculating the absolute errors of the HDF_{BSPM} with respect to the atrial HDF; an estimation was considered correct if the absolute error was ≤ 1 Hz. The spatial distribution of the errors between torso DFs and atrial HDFs were analyzed qualitatively based on the location of the driving mechanisms inside the atria (LA or RA). Torso HDF regions, defined as portions of the maps with $|DF - HDF_{BSPM}| \leq 0.5$ Hz, were identified and the percentage of the torso occupied these regions was compared between methods.

DF maps generated with both methods were compared in order to evaluate the effects of the wavelet approach in the DF distributions on the torso. The similarity between the maps was assessed with two-dimensional Pearson's correlation:

$$R = \frac{\sum_m \sum_n (W_{mn} - \mu_W)(M_{mn} - \mu_M)}{\sqrt{\sum_m \sum_n (W_{mn} - \mu_W)^2} \sqrt{\sum_m \sum_n (M_{mn} - \mu_M)^2}} \tag{3}$$

where W and M are DF maps obtained with the wavelet and Welch methods, m and n are matrix indexes and μ represents mean values.

2.6 Robustness of the method to noise and reduction in spatial resolution

The robustness of the atrial HDF estimations by the HDF_{BSPM} of the wavelet method to noise was evaluated under the presence of two different added artifacts: white Gaussian noise and a sinusoidal wave with frequency corresponding to the first harmonic of the atrial HDF (here called harmonic noise). The signal was contaminated with these artifacts with SNRs of 60, 30, 10, 5 and 1

dB and the absolute errors in atrial HDF estimation were used to quantify the effects of the increasing noise. The analyses were expanded to the Welch approach aiming to observe the ability of both methods to estimate the atrial HDF. Additionally, to evaluate the robustness of both methods to lower spatial resolution BSPM lead layouts, the analyses of AF models was reproduced for subsets of the 567 points used for the analyses of computer models (here denominated high-resolution layout - HR) with various numbers of leads: 256 [27], 127[10], 67[9], 64[28], 32 and 16 (Supplementary Fig. 1). For patient data, only the 32 and 16 lead layouts were used for comparison with the original 67 leads layout.

DF maps generated with both the wavelet and Welch methods in all lead layouts were compared with their HR counterpart using two-dimensional Pearson's correlation. Atrial HDF estimations were compared based on the absolute errors between the atrial and torso HDFs. Patterns of spatial distribution were qualitatively compared along lead layouts.

2.7 Statistical analysis

The normality of the data and homogeneity of variances were tested using Anderson-Darling and Bartlett's test, respectively. When the data followed these criteria, paired t-tests were used to compare results from different methods or lead layouts; otherwise, Wilcoxon signed-rank test was used. For comparing results from multiple groups measuring the same parameters (such as with different levels of noise or layouts), Friedman test was used (post-hoc: Nemenyi test); the null-hypothesis of the test is that the measurements with different settings are compatible with each other. Significance for all tests was set at $p < 0.05$.

3 Results

3.1 AF models

3.1.1 Estimation of the atrial HDF

Fig. 2A shows a typical example of a torso DF map calculated by the Welch and the proposed wavelet-based method on a patient with the HDF in the RA. It is of note that DF maps obtained with Welch periodograms present sharper transitions between DF values than in the wavelet method, where the transitions are gradual, resulting in a smoother map. In Fig. 2B we

can observe a signal from a region where a spurious HDF was detected in the Welch method. Although there are several inflections in the signal, only the main repetitive pattern is detected by the wavelet approach. The bottom of Fig. 2B shows how the HDF_{BSPM} obtained by the wavelet method is closer to the atrial HDF, whereas the Welch method detects a higher harmonic peak. Fig. 2C shows an excerpt of an EGM and a BSPM signal from the HDF region in the corresponding map, as marked with a square in Fig. 2A. It is possible to notice that periodicity detected by the wavelet method in the BSPM signal matches the one observed between the activation times in the EGM signal, as marked by the red dots.

Considering all AF simulations, the wavelet method performed better than the Welch approach in approximating the atrial HDF with HDF_{BSPM}, with an relative error $(median\ [IQR])$ of 7.14 [3.06 ~ 16.23]% (0.40 [0.20 ~ 1.13] Hz) vs. 60.00 [6.03 ~ 69.36]% (3.30 [0.35 ~ 4.15] Hz), $p = 0.06$ (Fig. 2D). Overall, the wavelet method resulted in correct estimations of atrial HDFs in 81.82% of the simulations, against 45.45% for Welch's estimates (Fig. 2E). DF maps presented low positive correlation between methods $(mean \pm std$: 0.47 ± 0.19, Fig. 2F), indicating important differences in the DF distributions between methods.

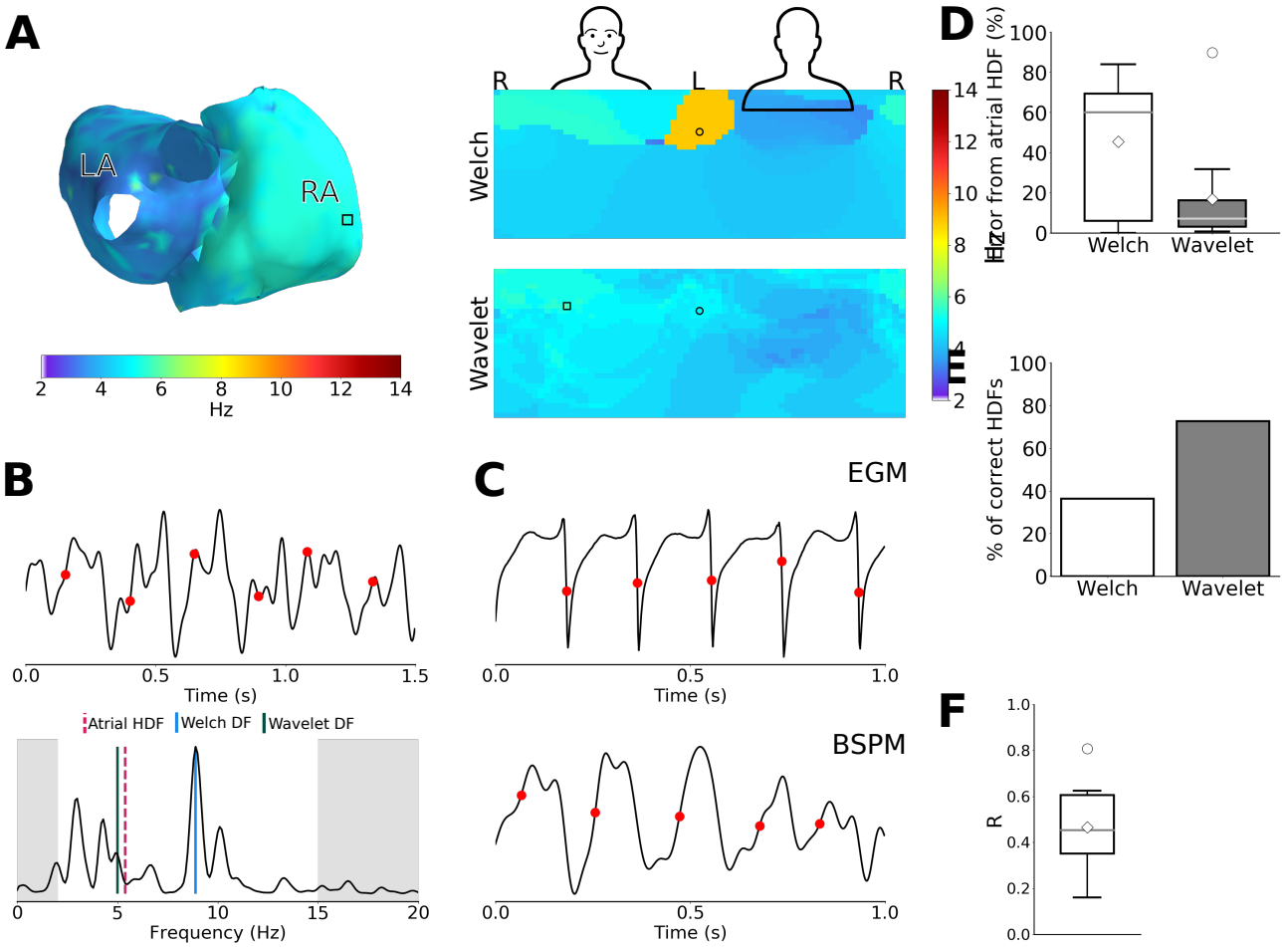

Figure 2: Example of changes in the DF maps with the Welch and wavelet methods from a model with the driver region in the RA. **A:** DF maps of the atria (left) and on the torso (right); torso maps were determined with the Welch (top) and wavelet (bottom) methods (right). It is possible to notice that the wavelet method presents smoother transitions between DFs than those observed in the Welch DF maps. **B:** Segment of the signal at the lead marked with a black circle in A and the respective Welch periodogram. The red dots mark the activations as detected by the wavelet method. Only the main patterns are detected with this method, with the smaller, noisy inflections being ignored. While the DF detected by the Welch method is a harmonic of another frequency in the spectrum, the wavelet method identifies a DF closer to the atrial HDF. **C:** Comparison between a segment of an EGM and a BSPM signal from the HDF regions, marked with a square in A. The periodicity detected by the wavelet method in the BSPM signal matches the number of activations observed in the EGM, as marked in red. **D:** Absolute percentage error in atrial HDF estimation with the HDF_{BSPM} for all simulations. Mean and median values are depicted as diamonds and lines, respectively, while circles are outliers. The wavelet method consistently achieves smaller errors than the Welch approach. **E:** Percentage of simulations with absolute errors from the atrial HDF ≤ 1 Hz (i.e. correct estimations of the atrial HDF) for both methods. **F:** 2D correlation coefficient between DF maps obtained with the wavelet and Welch methods for all simulations.

Fig. 3A shows the spatial distribution of absolute errors between atrial and BSPM HDF along the torso for two separate groups depending on which atrium was harboring the rotors and highest DF sites. While similarities were found between methods, the patterns observed present differences in the position of the regions with the smallest errors. For drivers in the LA, the lowest errors were observed on the posterior torso for both methods, mostly on the superior portion for

the Welch method and on the left inferior portion for the wavelet method. For drivers in the RA, errors were smaller on the anterior torso for both methods, especially for wavelet. Fig. 3B indicates that the wavelet method is either better or equivalent to the Welch approach in the majority of the torso, helping highlight the above-mentioned patterns. The percentage of the torso with $|DFs - \mathrm{HDF}_{BSPM}| \leq 0.5Hz$ was statistically equivalent between the Welch and wavelet methods (2.25[1.51 ~ 5.62] vs 5.43[3.49 ~ 5.62] %, respectively, $p = 0.53$)

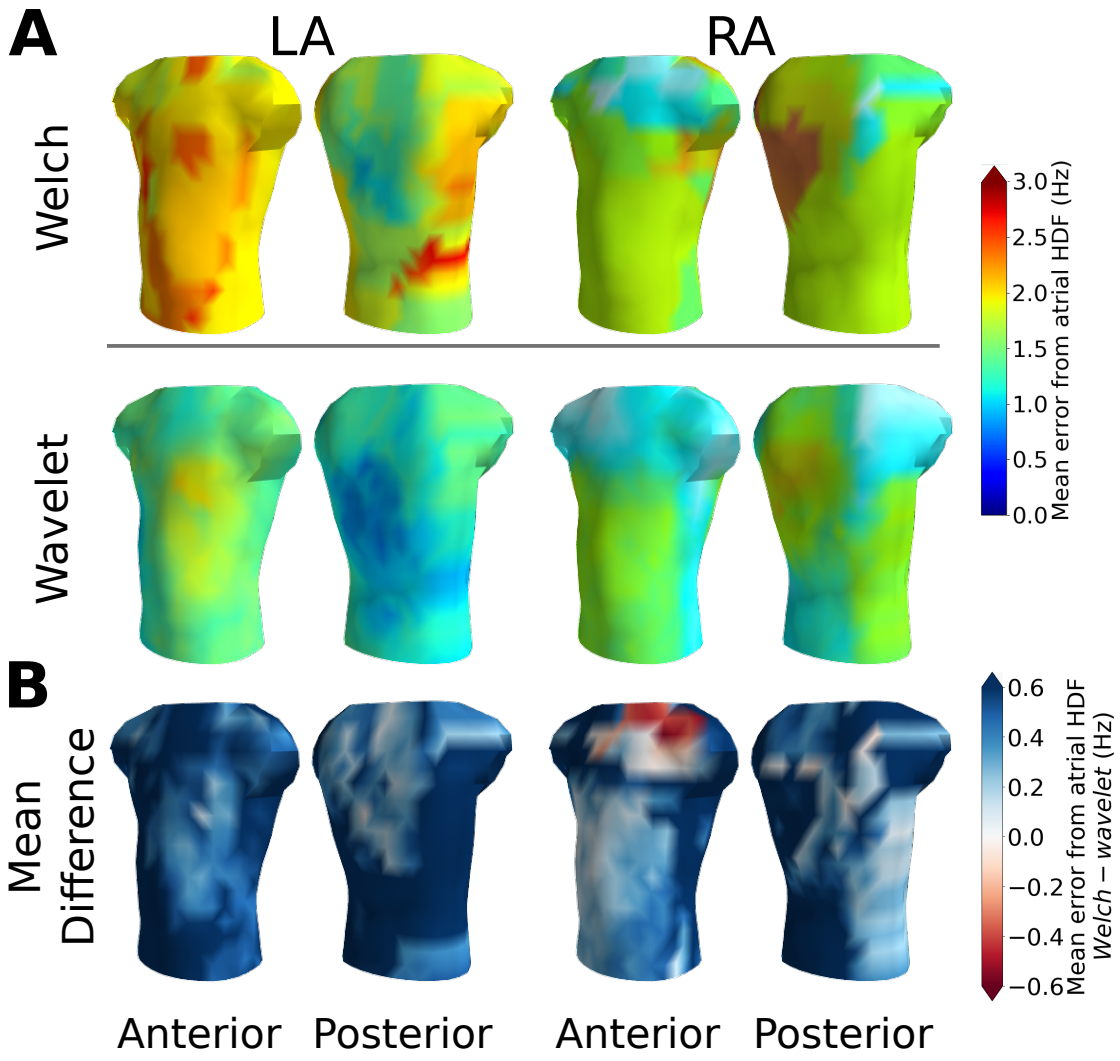

Figure 3: Spatial distribution of absolute errors on the torso for models with respect to the atrial HDF, divided by the atrium where the driver was located. **A:** Absolute differences between torso DFs obtained by both methods and atrial HDF. **B:** Mean difference between the errors from the atrial HDF obtained by both methods. Blue regions indicate portions of the torso where the wavelet performed better (i.e. Welch had higher average errors); in red regions, the Welch method performed better and in white regions, both methods were equivalent. The maps show that the wavelet method achieves lower errors in the majority of the torso. This helps to highlight patterns related to the location of the driving mechanism, such as the predominance of lower errors on the anterior torso for drivers in the RA and on the posterior torso for drivers on the LA.

3.1.2 Effects of noise and reduction in the number of leads

Fig. 4 summarizes the effects of the addition of white Gaussian noise (Fig. 4A), of sinusoidal waves at the harmonics of the atrial HDF (Fig. 4B) and of reducing the number of leads in atrial HDF estimation (Fig. 4C). The wavelet method is robust against Gaussian and harmonic noise, achieving lower mean and median errors than the Welch approach in every scenario. Significant differences in the estimations of the atrial HDF appeared for the wavelet method between the 1 dB and the 30 and 60 dB SNRs for the harmonic noise ($p < 0.01$). For the Welch method, significant differences appeared only with harmonic noise between the 1 dB and the 60 and 30 dB SNRs ($p < 0.05$).

Both Welch and wavelet approaches allow identifying the HDF even when reducing the amount of recorded leads from 567 to 16. Both methods achieve similar results along all lead layouts, with no significant differences ($p = 0.23$ and $p = 0.33$ for Welch and wavelet methods, respectively). Again, the errors obtained with the wavelet method are consistently lower than those obtained with the Welch periodograms. DF maps obtained in layouts with fewer leads correlated better with those from the HR configuration in the wavelet method than in the Welch. The spatial distribution of the differences from the atrial HDF for all lead layouts and both methods is displayed in Supplementary Fig. 2. Global patterns are consistent in both methods for all but the 32 and 16 lead layouts, where major differences appear especially in the simulations from the LA.

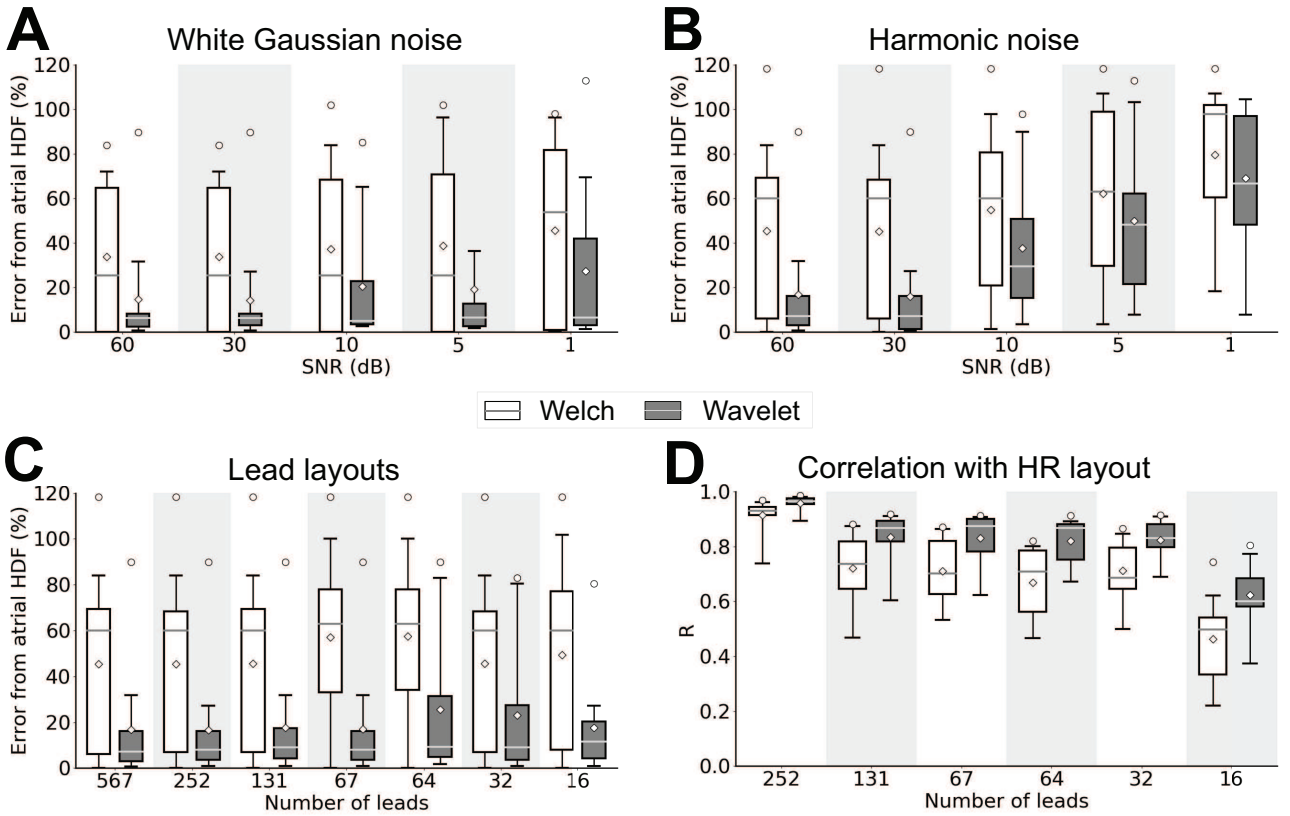

Figure 4: Robustness of the Welch and wavelet methods to uncertainties. **A:** White Gaussian noise with different SNRs. **B:** Harmonic noise with different SNRs. **C:** Reduction in the number of leads. The 2D correlation coefficient between DF maps obtained with the different lead layouts and their HR equivalent is displayed in **D** for all simulations. The wavelet method outperforms the Welch approach in almost every scenario, presenting higher correlation between maps along the lead layouts.

3.2 Patients

3.2.1 Estimation of atrial HDF

Fig. 5A-D gives an example of how the wavelet method can improve the result from Welch analysis in patients. The comparison of DF maps generated by both methods (Fig. 5A) shows a smoother map with the wavelet method, which contains a region of high DFs that do not appear in the Welch map. Looking at segments obtained from the HDF region in the atria (Fig. 5B) and in the BSPM (Fig. 5C), it is possible to observe that the activation times detected by the wavelet method correspond to the most prominent repetitive patterns, detecting cycle lengths similar to those observed in the EGMs. The DF estimates based on the activations is closer to the atrial HDF, while a higher peak in the spectrogram, unrelated to the atrial HDF, increases the error in the Welch method (Fig. 5D).

Analyses were expanded for all AF patients, showing that the atrial HDF estimated in patients

achieved an absolute error of 8.10 [5.50 ~ 13.14]% (0.75 [0.69 ~ 1.06] Hz) for the wavelet method in contrast to the 7.47 [5.59 ~ 19.62]% (0.72 [0.98 ~ 1.98] Hz) obtained by the Welch approach ($p = 0.06$,Fig. 5D). These errors resulted in correct estimations of atrial HDFs in 75.00% of the patients with the wavelet methodology, against 66.67% in the Welch estimates (Fig. 5E). The DF maps obtained with the different methods were more similar than in the models, with a 2D correlation coefficient of 0.63 ± 0.17 (Fig. 5F).

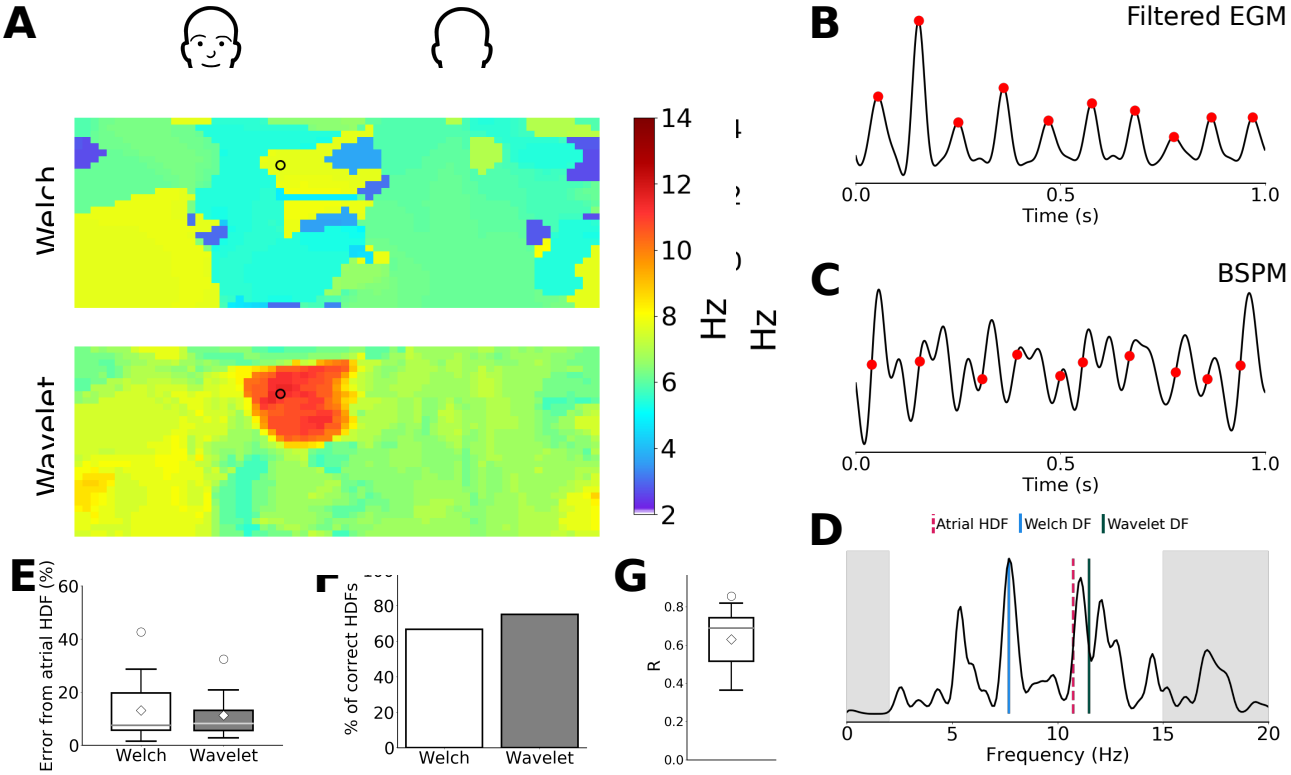

Figure 5: Example of the effect of the wavelet method in comparison to the Welch approach. **A:** DF maps from a patient with atrial HDF of 10.75 Hz in the LA obtained with the Welch (top) and wavelet (bottom) methods. A region with high DFs appears only in the wavelet map. **B:** Filtered EGM signal obtained from the HDF site in the RA **C:** Segment of a signal from the lead marked with a black circle in A. The red dots mark the activation times detected by the wavelet method. It is possible to observe that the periodicity observed in the signals from B and C are similar, indicating good correspondence between the activation times in the EGM and the detections by the wavelet method. **D:** Welch periodogram of the signal in B; peaks in shaded areas are ignored for the DF detection. The DF estimated with the wavelet method is close to the atrial HDF, while a higher peak prevents the detection of the proper DF in the Welch method. **D:** Absolute percentage error in atrial HDF estimation for all patients. Mean and median values are depicted as diamonds and lines, respectively, while circles are outliers. **E:** Percentage of patients with absolute errors from the atrial HDF ≤ 1 Hz (i.e. correct estimations of the atrial HDF) for both methods. **F:** 2D correlation coefficient between DF maps obtained with the wavelet and Welch methods for all patients.

The spatial distribution of the errors from the atrial HDF along the torso is displayed in Fig. 6. In patients with the driver in the LA, distributions were similar along the torso for the Welch method, but revealed lower errors on the anterior portion, especially on the left, for the wavelet approach. For the drivers in the RA, errors were higher on the posterior portion of the torso for

both methods, with the lower errors occurring on the right anterior portion of the torso. The errors with the wavelet method were either equivalent to or lower than those from the Welch approach along all the torso drivers in both atria. The portion of the torso with $|DFs - \text{HDF}_{BSPM}| \leq 0.5Hz$ was significantly different for both methods, occupying $13.41 \pm 7.28\%$ and $3.56 \pm 5.15\%$ of the torso in the Welch and wavelet methods, respectively ($p < 0.01$).

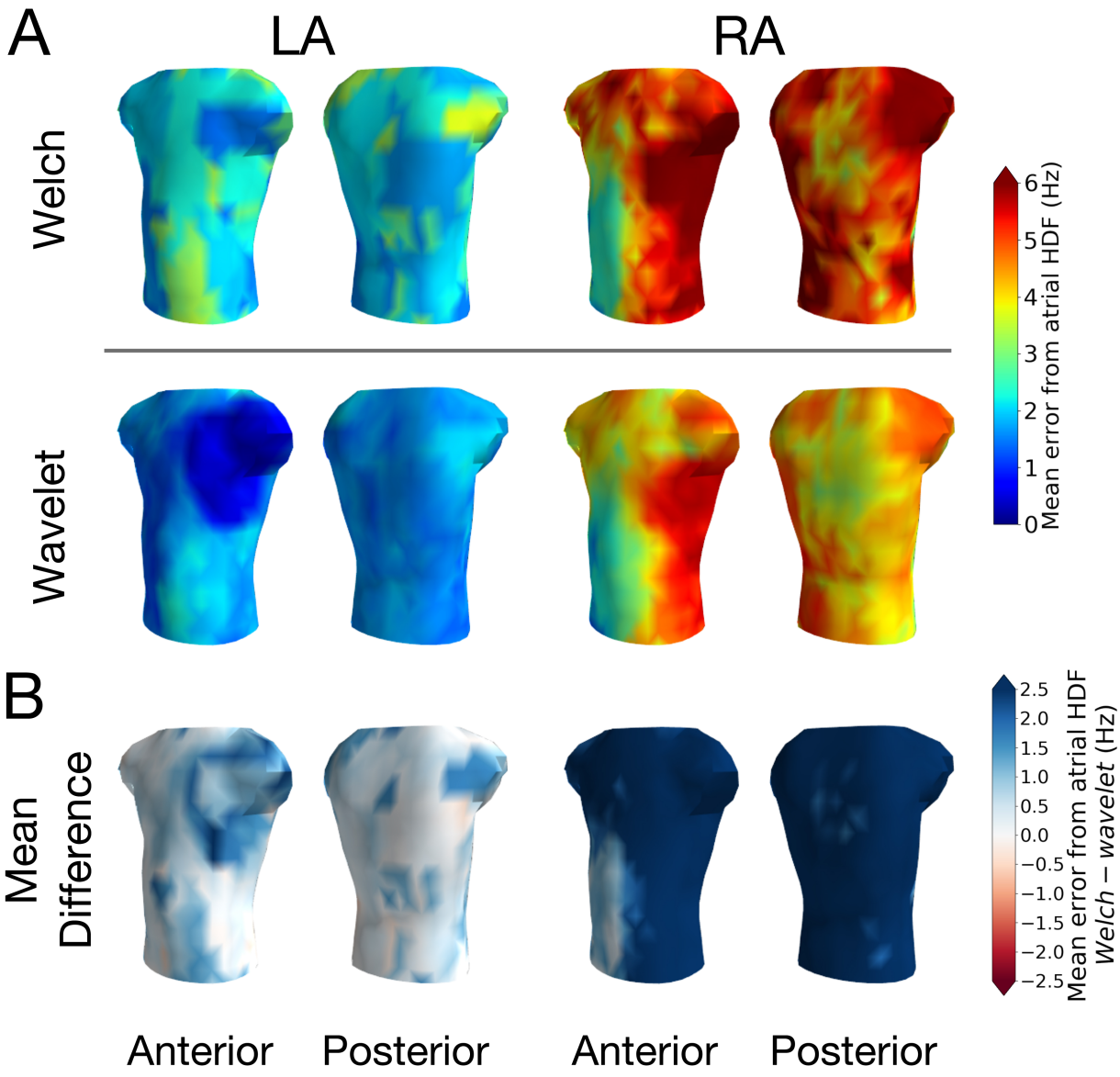

Figure 6: Spatial distribution of absolute errors on the torso for patients with respect to the atrial HDF, divided by the atrium where the driver was located. **A:** Absolute differences between torso DFs obtained by both methods and atrial HDF. **B:** Mean difference between the errors from the atrial HDF obtained by both methods. Blue regions indicate portions of the torso where the wavelet performed better (i.e. Welch had higher average errors); in red regions, the Welch method performed better and in white regions, both methods were equivalent. Errors are either lower or equivalent in the wavelet method when compared with the Welch approach. In the wavelet method, for patients with the driver in the RA, lower errors appear on the anterior portion of the torso, with a clear gradient to the posterior portion. For drivers in the LA, errors are lower on the left portion of the torso.

3.2.2 Effects of reduction in the number of leads

Fig. 7 shows the effect of reducing the number of leads in patient data from 67 leads down to 32 and 16 leads in atrial HDF estimation (Fig. 7A), as well as the correlation between DF maps generated with the reduced layouts in comparison to the original 67 leads (Fig. 7B). There were no significant differences between the atrial HDF estimated with the HDF_{BSPM} for both methods ($p = 0.43$ and $p = 0.79$ for Welch and wavelet, respectively). The spatial distribution in DF maps presented an intermediate positive correlation; when analyzing the spatial distribution of differences from the atrial HDF (Supplementary Fig. 3), the layouts with reduced numbers of leads present similar patterns than the original configuration, but less spatially localized.

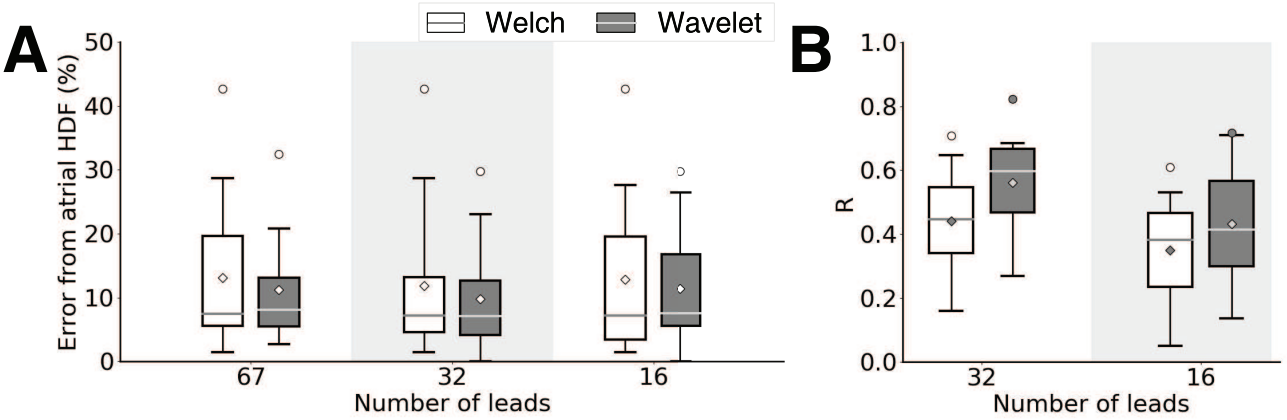

Figure 7: Effects of reducing the number of leads in patient data in outcomes from the Welch and wavelet methods. **A:** Absolute percentage error in atrial HDF estimation. **B:** Correlation between DF maps generated with the original and reduced number of leads

4 Discussion

In this study, a method based on maximum detection in continuous wavelet transform with Gaussian wavelets for the estimation of the DF in BSPM signals has been developed. Since there is no gold standard methodology for non-invasive DF estimation, comparisons were made with the traditional widely applied approach based on peak detection in Welch periodograms. From the results it can be highlighted that the proposed wavelet-based method showed a better accuracy for estimating the arrhythmic mechanism frequency, even under noisy conditions and relative low number of layout leads.

DF analysis has been introduced in the study of the AF dynamics as a means to provide an alternative to the annotation of activations in EGMs, allowing a reliable periodicity measurement of

fibrillatory waves that is more robust to amplitude and morphology changes than manual or automated time analysis [13], [16]. However, frequency analysis is subject to some uncertainties that may significantly alter the resulting DF, such as variation in amplitude, frequency or phase, fractionation, and ventricular influence [13], [16]. Although parallel observation of signals in the time domain may mitigate some of these issues [13], manual correction of the results may be needed to avoid the detection of harmonic DFs and exclusion of noisy leads [9], [10].

Wavelet transform is an intermediary technique between pure time or frequency analyses, providing good localization in both domains [18]. Our methodology incorporates characteristics of both traditional time and frequency analyses into a single approach: the selection of the scale with the highest energy in the AF physiological range acts as a sort of "DF" selection, focusing on the dominant periodic characteristics, but not restricting the analysis to a single frequency component. Using a first-order Gaussian wavelet to perform CWT provides a reliable method for obtaining activation times based on the identification of points with close to singular behavior (i.e. sharp transitions). This avoids the use of derivative-based detection of activations [5], which has an intrinsic high-pass characteristic and might lead to double counting due to the multiple inflections of the AF signal [19].

In this work, comparison with Welch's periodogram method for approximating the atrial HDF indicated that our approach obtains consistently lower errors even in situations with low SNR and with limited lead layouts. Differences in performance between the Wavelet-based method and Welch periodogram are smaller for the patient group compared to modeled AF (75.00% vs 66.67% and 81.82% vs 45.45% respectively). The promising results on mathematical models highlight the usefulness of the proposed technique, although further analyses are required on a larger dataset of patients to validate the statistical significance.

In other studies, the correspondence between surface HDF estimated with Welch periodograms and atrial HDF was stronger than in the results presented here [9], [10]. However, in the mentioned studies, visual inspection of the quality of the signals and/or of the peak detection in the periodograms was conducted, leading to the manual exclusion of problematic leads; this step was not performed in the current study. This allowed for the comparison of both methods in a purely automatic configuration. In this scenario, our results indicate that the wavelet method for DF detection is more suited to unsupervised applications, such as clinical decision support systems.

Correlation between DF maps obtained with the Welch and the wavelet methods suggested the presence of relevant differences in the spatial distribution of DFs. Observation of the DF maps (see Supplementary Figs. 4 and 5) indicates that most of the maps present a global similarity, with regions of similar frequencies appearing in approximately in the same positions even in low correlation cases (e.g. models 2, 3 and 9 and most of the patients). However, the sizes of the regions vary considerably and some HDF_{BSPM} regions appear in different positions, usually due to noisy HDF detections (e.g. models 2, 6 and 11).

Previous studies have evaluated the spatial distribution of DFs and their relationship to the atrial DF patterns [9], [29], [30]. HDFs appearing on the left and posterior portions of the torso correlated better with atrial HDFs inside the LA, whereas HDFs in the RA reflected in BSPM HDFs on the anterior and right portions of the torso [9], [29]. These patterns have been observed here for both methods when analyzing the spatial distribution of errors in atrial HDF estimation; however, the wavelet method presented in average smaller absolute errors in most of the torso. This resulted in clearer error gradients for this method, helping highlight the predominance of lower errors on the anterior torso for drivers in the RA vs. on the posterior torso for drivers in the LA. Further studies with spatially detailed invasive measurements are needed to validate whether the locations of the HDF_{BSPM} in the wavelet method increase the ability of the BSPM to approximate atrial DF distributions.

In addition to the above-mentioned improvements in DF analysis for AF, the proposed methodology also has the potential to aid studies in the time and phase domains. The propagation of activation wavefronts can be used for the non-invasive study of AF patterns [5] and is addressed by our methodology, which relies on activation times for DF estimation. Although the precise marking of AF wavefronts can be a difficult task in BSPM due to the multiple inflections of the fibrillatory waves, the method proposed here delivers consistent estimations of these points, that could be used to improve other time-based analysis such as those presented in [5] and [6].

In phase analysis, precise and/or time-specific detection of DFs is essential for conditioning signals before applying the Hilbert transform, be that by narrow band-pass filtering around the DF to stabilize the rotational activity [7] or for detrending the signals to achieve more consistent results [19]. Since our methodology identifies individual waves in the BSPM signals and estimates each CL, instantaneous DF estimation is possible and can be used in more sophisticated phase

analysis algorithms. Additionally, the errors in DF estimation with respect to the atrial HDF were smaller, which guarantees that the narrow band-pass filtering is focusing the analyses in the frequencies truly related to the rotors.

5 Study limitations

In this study, a limited number of 11 simulations and 12 patients with AF were used to validate the methodology. This number may not account for the complexity and variability of AF in the general population and the methodology should be further validated in larger data sets. The AF models were contaminated with white Gaussian noise, but it might not represent all forms of noise collected during clinical studies with non-invasive cardiac recordings. Although the Welch approach has been a widely applied method for estimating DF from BSPM maps, and that the present study proposed a method that does perform better, it should be emphasized that currently there is no gold standard method for estimating DF from BSPM maps.

Patient data were recorded under adenosine infusion, which speeds-up the atrial activation frequency in a way that might not be present in basal AF, resulting in higher atrial HDFs. This paper does not address the effects on DF estimation after ventricular far-field cancellation on the AF body surface signals.

6 Conclusion

Estimations of atrial HDFs using BSPM can be improved by the use of the continuous wavelet transform based algorithm presented in this work. More precise estimations can enhance the diagnostic ability of the DF analyses in BSPM and may improve the outcomes of time or phase analyses, increasing the value of the BSPM as a low complexity tool for early diagnosis and follow-up.

7 Acknowledgments

This study was supported in part by grants from São Paulo Research Foundation (2017/19775-3), Instituto de Salud Carlos III FEDER (Fondo Europeo de Desarrollo Regional PI17/01106) and Generalitat Valenciana Grants (AICO/2018/267).

Disclosures: M. S. Guillem is shareholder of Corify Care S.L.

References

[1] P. Kirchhof, S. Benussi, D. Kotecha, A. Ahlsson, D. Atar, B. Casadei, M. Castella, H.-C. Diener, H. Heidbuchel, J. Hendriks, *et al.*, "2016 esc guidelines for the management of atrial fibrillation developed in collaboration with eacts", *European journal of cardio-thoracic surgery*, vol. 50, no. 5, e1–e88, 2016.

[2] F. Atienza, J. Almendral, J. M. Ormaetxe, Á. Moya, J. D. Martínez-Alday, A. Hernández-Madrid, E. Castellanos, F. Arribas, M. Á. Arias, L. Tercedor, *et al.*, "Comparison of radiofrequency catheter ablation of drivers and circumferential pulmonary vein isolation in atrial fibrillation: A noninferiority randomized multicenter radar-af trial", *Journal of the American College of Cardiology*, vol. 64, no. 23, pp. 2455–2467, 2014.

[3] S. M. Narayan, D. E. Krummen, K. Shivkumar, P. Clopton, W.-J. Rappel, and J. M. Miller, "Treatment of atrial fibrillation by the ablation of localized sources: CONFIRM (conventional ablation for atrial fibrillation with or without focal impulse and rotor modulation) trial", *Journal of the American College of Cardiology*, vol. 60, no. 7, pp. 628–636, 2012.

[4] M. S. Guillem, A. M. Climent, M. Rodrigo, F. Fernández-Avilés, F. Atienza, and O. Berenfeld, "Presence and stability of rotors in atrial fibrillation: Evidence and therapeutic implications", *Cardiovascular research*, vol. 109, no. 4, pp. 480–492, 2016.

[5] M. S. Guillem, A. M. Climent, F. Castells, D. Husser, J. Millet, A. Arya, C. Piorkowski, and A. Bollmann, "Noninvasive mapping of human atrial fibrillation", *Journal of cardiovascular electrophysiology*, vol. 20, no. 5, pp. 507–513, 2009.

[6] E. A. P. Alday, M. A. Colman, P. Langley, and H. Zhang, "Novel non-invasive algorithm to identify the origins of re-entry and ectopic foci in the atria from 64-lead ecgs: A computational study", *PLoS computational biology*, vol. 13, no. 3, e1005270, 2017.

[7] M. Rodrigo, M. S. Guillem, A. M. Climent, J. Pedrón-Torrecilla, A. Liberos, J. Millet, F. Fernández-Avilés, F. Atienza, and O. Berenfeld, "Body surface localization of left and right atrial high-frequency rotors in atrial fibrillation patients: A clinical-computational study", *Heart Rhythm*, vol. 11, no. 9, pp. 1584–1591, 2014.

[8] C. Ramanathan, R. N. Ghanem, P. Jia, K. Ryu, and Y. Rudy, "Noninvasive electrocardiographic imaging for cardiac electrophysiology and arrhythmia", *Nature medicine*, vol. 10, no. 4, p. 422, 2004.

[9] M. S. Guillem, A. M. Climent, J. Millet, Á. Arenal, F. Fernández-Avilés, J. Jalife, F. Atienza, and O. Berenfeld, "Noninvasive localization of maximal frequency sites of atrial fibrillation by body surface potential mapping", *Circulation: Arrhythmia and Electrophysiology*, vol. 6, no. 2, pp. 294–301, 2013.

[10] F. J. Vanheusden, G. S. Chu, X. Li, J. Salinet, T. P. Almeida, N. Dastagir, P. J. Stafford, G. A. Ng, and F. S. Schlindwein, "Systematic differences of non-invasive dominant frequency estimation compared to invasive dominant frequency estimation in atrial fibrillation", *Computers in biology and medicine*, vol. 104, pp. 299–309, 2019.

[11] J. Jalife, O. Berenfeld, and M. Mansour, "Mother rotors and fibrillatory conduction: A mechanism of atrial fibrillation", *Cardiovascular research*, vol. 54, no. 2, pp. 204–216, 2002.

[12] P. Sanders, O. Berenfeld, M. Hocini, P. Jais, R. Vaidyanathan, L.-F. Hsu, S. Garrigue, Y. Takahashi, M. Rotter, F. Sacher, *et al.*, "Spectral analysis identifies sites of high-frequency activity maintaining atrial fibrillation in humans", *Circulation*, vol. 112, no. 6, pp. 789–797, 2005.

[13] J. Ng and J. J. Goldberger, "Understanding and interpreting dominant frequency analysis of af electrograms", *Journal of cardiovascular electrophysiology*, vol. 18, no. 6, pp. 680–685, 2007.

[14] F. Atienza, J. Almendral, J. Jalife, S. Zlochiver, R. Ploutz-Snyder, E. G. Torrecilla, A. Arenal, J. Kalifa, F. Fernández-Avilés, and O. Berenfeld, "Real-time dominant frequency mapping and ablation of dominant frequency sites in atrial fibrillation with left-to-right frequency gradients predicts long-term maintenance of sinus rhythm", *Heart Rhythm*, vol. 6, no. 1, pp. 33–40, 2009.

[15] X. Li, J. L. Salinet, T. P. Almeida, F. J. Vanheusden, G. S. Chu, G. A. Ng, and F. S. Schlindwein, "An interactive platform to guide catheter ablation in human persistent atrial fibrillation using dominant frequency, organization and phase mapping", *Computer methods and programs in biomedicine*, vol. 141, pp. 83–92, 2017.

[16] J. Ng, A. H. Kadish, and J. J. Goldberger, "Effect of electrogram characteristics on the relationship of dominant frequency to atrial activation rate in atrial fibrillation", *Heart Rhythm*, vol. 3, no. 11, pp. 1295–1305, 2006.

[17] I. Romero, E. Fleck, and C. Kriatselis, "Frequency analysis of atrial fibrillation surface and intracardiac electrograms during pulmonary vein isolation", *Europace*, vol. 13, no. 9, pp. 1340–1345, 2011.

[18] S. Mallat and W. L. Hwang, "Singularity detection and processing with wavelets", *IEEE transactions on information theory*, vol. 38, no. 2, pp. 617–643, 1992.

[19] R. Vijayakumar, S. K. Vasireddi, P. S. Cuculich, M. N. Faddis, and Y. Rudy, "Methodology considerations in phase mapping of human cardiac arrhythmias", *Circulation: Arrhythmia and Electrophysiology*, vol. 9, no. 11, e004409, 2016.

[20] M. W. Krueger, G. Seemann, K. Rhode, D. U. Keller, C. Schilling, A. Arujuna, J. Gill, M. D. O'Neill, R. Razavi, and O. Dossel, "Personalization of atrial anatomy and electrophysiology as a basis for clinical modeling of radio-frequency ablation of atrial fibrillation", *IEEE transactions on medical imaging*, vol. 32, no. 1, pp. 73–84, 2012.

[21] M. Rodrigo, A. M. Climent, A. Liberos, F. Fernández-Avilés, O. Berenfeld, F. Atienza, and M. S. Guillem, "Highest dominant frequency and rotor positions are robust markers of driver location during noninvasive mapping of atrial fibrillation: A computational study", *Heart rhythm*, vol. 14, no. 8, pp. 1224–1233, 2017.

[22] J. T. Koivumäki, G. Seemann, M. M. Maleckar, and P. Tavi, "In silico screening of the key cellular remodeling targets in chronic atrial fibrillation", *PLoS computational biology*, vol. 10, no. 5, e1003620, 2014.

[23] V. M. Garca-Molla, A. Liberos, A. Vidal, M. Guillem, J. Millet, A. Gonzalez, F.-J. Martnez-Zaldvar, and A. M. Climent, "Adaptive step ode algorithms for the 3d simulation of electric heart activity with graphics processing units", *Computers in biology and medicine*, vol. 44, pp. 15–26, 2014.

[24] M. Rodrigo, A. M. Climent, A. Liberos, F. Fernández-Avilés, O. Berenfeld, F. Atienza, and M. S. Guillem, "Technical considerations on phase mapping for identification of atrial reentrant

activity in direct-and inverse-computed electrograms", *Circulation: Arrhythmia and Electrophysiology*, vol. 10, no. 9, e005008, 2017.

[25] M. Guillem, A. Quesada, V. Donis, A. Climent, N. Mihi, J. Millet, and F. Castells, "Surface wavefront propagation maps: Non-invasive characterization of atrial flutter circuit", *Int J Bioelectromagn*, vol. 11, pp. 22–26, 2009.

[26] J. L. Salinet, J. H. Tuan, A. J. Sandilands, P. J. Stafford, F. S. Schlindwein, and G. A. Ng, "Distinctive patterns of dominant frequency trajectory behavior in drug-refractory persistent atrial fibrillation: Preliminary characterization of spatiotemporal instability", *Journal of cardiovascular electrophysiology*, vol. 25, no. 4, pp. 371–379, 2014.

[27] M. Haïssaguerre, M. Hocini, A. Denis, A. J. Shah, Y. Komatsu, S. Yamashita, M. Daly, S. Amraoui, S. Zellerhoff, M.-Q. Picat, *et al.*, "Driver domains in persistent atrial fibrillation", *Circulation*, vol. 130, no. 7, pp. 530–538, 2014.

[28] J. L. Salinet, V. G. Marques, M. Mazzetto, E. D. Camargo, C. A. Pastore, and I. A. Cestari, "A 64-lead body surface potential mapping system", in *2017 Computing in Cardiology (CinC)*, IEEE, 2017, pp. 1–4.

[29] M. Bojarnejad, J. R. Blake, J. Bourke, E. Shepherd, A. Murray, and P. Langley, "Non-invasive estimation of left atrial dominant frequency in atrial fibrillation from different electrode sites: Insight from body surface potential mapping", *Journal of atrial fibrillation*, vol. 7, no. 3, 2014.

[30] M. Rodrigo, A. Climent, A. Liberos, F. Fernández-Aviles, F. Atienza, M. Guillem, and O. Berenfeld, "Minimal configuration of body surface potential mapping for discrimination of left versus right dominant frequencies during atrial fibrillation", *Pacing and Clinical Electrophysiology*, vol. 40, no. 8, pp. 940–946, 2017.

A robust wavelet-based approach for dominant frequency analysis of atrial fibrillation in body surface signals

V. G. Marques[1], M. Rodrigo[2], M. S. Guillem[2], J. Salinet[1]

[1] Biomedical Engineering, Center for Engineering, Modeling and Applied Social Sciences, Federal University of ABC, Brazil

[2] ITACA Institute, Universitat Politècnica de València, Spain

Corresponding author:

João Salinet

Biomedical Engineering

Center for Engineering, Modeling and Applied Social Sciences (CECS)

Federal University of ABC, São Bernardo do Campo, São Paulo, Brazil

Address: Alameda da Universidade, s/n - Anchieta 09606-045

Email: joao.salinet@ufabc.edu.br

Phone: +55 11 2320 – 6342

ORCID: 0000-0003-2906-9397

Abstract

Objective: Atrial dominant frequency (DF) maps undergoing atrial fibrillation (AF) presented good spatial correlation with those obtained with the non-invasive body surface potential mapping (BSPM). In this study, a robust BSPM-DF calculation method based on wavelet analysis is proposed.

Approach: Continuous wavelet transform along 40 scales in the pseudo-frequency range of 3-30 Hz is performed in each BSPM signal using a Gaussian mother wavelet. DFs are estimated from the intervals between the peaks, representing the activation times, in the maximum energy scale. The results are compared with the traditionally widely applied Welch periodogram and the robustness was tested on different protocols: increasing levels of white Gaussian noise, artificial DF harmonics presence and reduction of number of leads. 11 AF simulations and 12 AF patients are considered in the analysis. For each patient, intracardiac electrograms were acquired in 15 locations from both atria. The accuracy of both methods was assessed by calculating the absolute errors of the HDF_{BSPM} with respect to the atrial HDF, either simulated or intracardially measured, and assumed correct if ≤ 1 Hz. The spatial distribution of the errors between torso DFs and atrial HDFs were compared with atria driving mechanisms location. Torso HDF regions, defined as portions of the maps with $|DF - \mathrm{HDF}_{BSPM}| \leq 0.5$ Hz were identified and the percentage of the torso occupied these regions was compared between methods.

Main results: The proposed method allowed a significant improvement on non-invasive estimation of the atria HDF (median relative error of 7.14% vs. 60.00%, p = 0.06), outperforming the Welch approach in correct estimations of atrial HDFs non-invasively for both cases: models (81.82% vs 45.45%) and patients (75.00% vs 66.67%). A low positive BSPM-DF maps correlation was seen between techniques (0.47 for models and 0.63 for patients), highlighting overall differences in DF distributions. The method was more robust to white Gaussian noise and harmonics and presented more consistent results in lead layouts with low spatial resolution ($p = 0.99$ vs. $p = 0.94$).

Significance: Estimation of atrial HDFs using BSPM is improved by the proposed wavelet-based algorithm, helping increase the non-invasive diagnostic ability in AF.

Keywords: atrial fibrillation, non-invasive, dominant frequency, wavelet, body surface potential mapping

1 Introduction

Atrial fibrillation (AF) is the most common cardiac arrhythmia in clinical practice, with an estimated prevalence of 3% in the population above 20 years, a percentage that tends to increase with the aging population [1]. AF is associated with high mortality and morbidity, mainly due to an increased risk of thromboembolic events such as strokes [1]. The mechanisms behind AF are complex and not yet completely understood [1]. Recent studies have related the maintenance of AF to localized regions, which can then be targeted for ablation, improving the therapy outcomes by following personalized approaches [2], [3]

Invasive electrophysiological studies, in which cardiac electrograms (EGMs) are measured directly in the atria using mapping catheters, are the most straightforward approach to identifying regions maintaining AF. However, this strategy is technically complex, demanding a large amount of time, resources and with risks for the patients, motivating the development of non-invasive methods [4]–[7], such as body surface potential mapping (BSPM) and electrocardiographic imaging (ECGi) [4]. Both these techniques are based on the measurement of electrocardiograms, which are then used to obtain information about the atrial behavior, either by directly analyzing the signals [4] or, with the aid of an imaging technique, by using inverse problem analysis and estimating epicardial (or endocardial) electrical activity [8]. Among these techniques, BSPM is the simplest approach, demanding relatively simple hardware and software to analyze the signals, and yielding relevant clinical results [6], [7], [9], which can be of use both in early diagnosis and follow-up [7], [10].

AF was traditionally thought to be maintained by disorganized conduction in the atria, with multiple wavelets that coexist and present no discernible pattern [11]. This view has been challenged by experiments both in animal models and patients, where spatiotemporally organized activity has been identified in the form of high-frequency sources (rotors and/or focal activity), which are thought to maintain the fibrillatory conduction [11], [12]. Locating these AF drivers relies on the identification of regions with a fast activation rate, but this is often a challenging task using time analysis of the complex AF EGMs [13]. Thus, researchers have migrated to analysis in the frequency domain in an attempt to overcome this barrier.

Researchers using spectral analysis have shown that AF signals have important periodic elements with varying degrees of regularity. It has also been shown that signals from certain regions

of the atria may have higher frequency components than those from other regions, suggesting that these areas may be the drivers that maintain AF and could be targets for ablation [11], [13]. It was noticed that the duration of the AF cycle in the left atrium (LA) correlates with the highest power peak of the related spectrum, defined as the dominant frequency (DF) [11]. DF analysis allowed to identify micro-reentries, discrete sites of periodic high-frequency activity responsible for AF maintenance [11], improving the current knowledge of this complex arrhythmia.

DF analysis of EGMs has led to the development of new ablation strategies that target high frequency regions in the atria [12], [14], [15]. Investigators using this approach achieved rates of success as high as 88% and 56% in paroxysmal and persistent AF, respectively [14], and managed to reduce the frequency gradient between the left and right atria, related to the maintenance and recurrence of the arrhythmia [14]. Recently, investigators showed that the highest DF (HDF) areas responsible for AF maintenance can be identified non-invasively through the BSPM DF mapping [9], even with the low-pass filter effect intrinsically related to the volume conductor effect present within the heart and torso [10], providing a valuable clinical tool which can be used prior invasive mapping. Therefore, it is important for new studies to check whether the clinically useful parameter (atrial HDF) can also be precisely detected on the torso. Moreover, since there is no gold standard methodology for non-invasive DF estimation, researchers made use of the widely applied approach based on peak detection in Welch periodograms.

Nonetheless, Fourier based DF analysis presents important limitations, such as the lack of the identification of specific activation times and sensitivity to signal uncertainties such as the presence of harmonic activity and dynamic changes in frequency and phase [13], [16]. Although parallel observation of time signals can mitigate some of these issues [13], a more robust solution is desirable for automatic applications.

A possible alternative for traditional Fourier based DF analysis is using wavelet transform, which can be understood as a generalization of the Fourier transform in which the sine waves are replaced by stretched, squeezed and translated versions of a single waveform, called mother wavelet [17]. The signal is then decomposed in scales rather than frequencies, which are related to a bandwidth, depending on the chosen wavelet. Wavelet transform is a technique with good localization in both time and frequency domains and has the ability to identify points with close to singular behavior [18], such as the sharp transitions associated with activations in BSPM. Pre-

vious studies have used wavelet transforms in the analysis of AF signals, but have been focused in reconstructed epicardial signals rather than in BSPM [19] or have performed analyses based on the energy of scales rather than identified activations [17].

In this study, we proposed a wavelet-based method for estimating atrial HDFs based on the identification of individual activation times. This technique outperformed the Welch periodogram for estimating non-invasively the frequency activity of the AF mechanism, even under noisy conditions, harmonic activity and relative low number of leads in the BSPM layout.

2 Methods

2.1 AF models

A realistic 3D model of the atrial anatomy composed by 284,578 nodes and 1,353,783 tetrahedrons ($673.4 \pm 130.3 \mu m$ between nodes)[20], [21] was used to simulate the atrial electrical activity. A gradient on the electrophysiological properties of the atrial myocardium, specifically on I_{K1}, I_{Na} and I_{CaL} [22], was introduced into the atrial cell formulation [22] to obtain AF propagation patterns maintained by rotors and with spatial variations in the activation rate. Fibrotic tissue was modeled by electrically disconnecting a spatial random amount between 20% and 60% of the total nodes in order to create AF patterns with dominant regions with different shape and extension. The system of differential equations in the atrial cell model was solved by using Runge-Kutta integration based on a graphic processors unit (NVIDIA Tesla C2075 6G) [23]. The stimulation protocol for rotor formation consisted in a S1S2 protocol, with a plane S1 wave and a square S2 wave.

An ensemble of 11 rotor driven AF simulations with 4 seconds each and localized in different portions of the LA and right atrium (RA) were used for the analyses [24]. An uniform mesh (2048 points, 0.51 ± 0.26 cm between nodes) of unipolar EGMs obtained with the models were preprocessed as described elsewhere [24] and DF values were determined in each of the EGMs by detecting the highest power peak in Welch periodograms (80% overlap, zero-padded to achieve a spectral resolution of 0.01 Hz)[9], [24]. DF values were manually inspected and compared with the activation counts to avoid inconsistent detections. The atrial HDF at the location of the functional rotor was defined as the driving frequency of AF. Table 1 summarizes the details of the simulations.

Table 1: Characteristics of the simulations

Model	Rotor location	Atrial HDF (Hz)
1	LA	4.80
2	LA	5.60
3	Left inferior pulmonary vein (LA)	5.50
4	Left superior pulmonary vein (LA)	7.80
5	RA	7.60
6	RA	5.40
7	RA appendage	5.80
8	RA appendage	5.80
9	Right inferior pulmonary vein (LA)	5.50
10	Right inferior pulmonary vein (LA)	5.40
11	Right superior pulmonary vein (LA)	6.80

LA: left atrium; RA: right atrium

BSPM signals were obtained by solving the forward problem with the boundary element method, resulting in 771 nodes with signals referenced to the Wilson central terminal and sampled at f_S = 500 Hz [24], of which 567 points were selected to represent leads of a realistic measurement, excluding points inside the waist, neck or arms. White Gaussian noise was added to the BSPM signals with a signal-to-noise ratio (SNR) of 60 dB[24].

2.2 Patient data

67 BSPM leads were recorded on the torso from 12 patients admitted for ablation of drug-refractory paroxysmal and persistent AF (Table 2) [9]. Simultaneously, intracardiac EGMs were acquired in 15 locations from both atria (f_S = 977 Hz) [9]: the following catheters were introduced via the right femoral vein: (1) a standard tetrapolar catheter in the RA appendage; (2) a deflectable 4-mm mapping catheter (Marinr; Medtronic Inc., Minneapolis, MN) in the distal coronary sinus; (3) a decapolar circular mapping Lasso catheter (Biosense-Webster, Diamond Bar, CA) used to map the pulmonary veins LA junctions; and (4) a Navistar catheter (3.5-mm tip, 2-5-2 interelectrode

distance; Thermo-Cool, Biosense-Webster, Diamond Bar, CA). Bipolar atrial EGMs were recorded by using the CARTO navigation system with embedded spectral analysis capabilities (CARTO XP, version 7.7; Biosense-Webster, Diamond Bar, CA). Signals were then band-pass filtered (40 - 250 Hz), rectified, and then low-pass filtered (20 Hz).

4-second segments within the longest RR interval after the administration of adenosine were used for the analysis of atrial EGMs and BSPM. In 3 patients, QRS complexes were canceled, as the RR intervals were shorter than 4 seconds. DFs in atrial EGMs were determined in each location by detecting the peak with the highest frequency power in Welch periodograms [11]. To avoid inconsistencies, the local activations were detected and manually inspected simultaneously to the DF estimation of atrial signals by Welch, allowing the frequency of activations to be obtained. The atrial HDF was determined and its location was defined as the main driving region of the arrhythmia in the patients (Table 2).

Table 2: Characteristics of the patients

Patient	Age	Gender	AF type	Atrial HDF (Hz)	HDF location
1	47	M	Paroxysmal	10.75	RA
2	54	M	Paroxysmal	10.25	LA
3	64	M	Paroxysmal	13.25	RA
4	49	M	Paroxysmal	9.75	RA
5	51	M	Paroxysmal	10.00	RA
6	60	M	Persistent	10.00	RA
7	61	M	Paroxysmal	9.25	RA
8	47	M	Persistent	9.25	RA
9	59	M	Persistent	6.50	LA
10	68	F	Paroxysmal	11.50	RA
11	67	M	Paroxysmal	6.00	RA
12	47	M	Paroxysmal	7.00	LA

F: female; M: male; LA: left atrium; RA: right atrium

2.3 Preprocessing of BSPM signals

The three-dimensional coordinates of the BSPM nodes in the models were mapped to a two-dimensional configuration by projecting their positions into a cylinder wall. This cylinder has the same height as the torso (61.5 cm) and is centered at the barycenter of the coordinates from all BSPM nodes; the radius is the largest horizontal distance between any point and the center of the cylinder (22.5 cm). The cylinder was unwrapped to a rectangle with the left side of the torso at the center. Electrode positions in patients were arranged in a two-dimensional configuration based on the lead layout (Supplementary Fig. 1); distances between adjacent electrode columns and rows were set at 5 cm. The signals from both models and patients were interpolated into a 30 X 65 grid using cubic splines.

Filtering was performed, when indicated in the methodology, as following: the baseline was estimated by downsampling the signal to $0.025 \cdot f_S$ Hz and low-pass filtering at 0.5 Hz (10th order Butterworth). Baseline signals were then interpolated to their initial f_S and subtracted from the original signals [5]. A low-pass filter (10th order Butterworth) was applied at 30 Hz, covering the spectral range of AF [5].

2.4 DF detection on surface signals

DFs were estimated using a method based on continuous wavelet transform (CWT) modulus maxima detection [19]. When CWT is performed using a wavelet that is the derivative of a smooth function, the extreme points on the results correspond to sharp deflections on the original signal, similar to singularities [18]. This characteristic can be used to detect sharp deflections on BSPM, associated with depolarization wavefronts [25].

Thus, for each lead, CWT was applied on the unfiltered signals using a negative first-order Gaussian mother wavelet (Eq. 1, where C is a normalization constant so that the L2-norm of ψ is equal to 1) along 40 linearly spaced scales in the pseudo-frequency range of 3 to 30 Hz. In order to detect the most physiologically relevant positive deflections, the scale with the highest energy was selected for further processing (Eq. 2, where n are indexes, a are scales and W_a is the CWT of the signal at that scale); the rationale is that this scale contains the most information about a signal and thus represents better its main properties, such as the activation patterns in a BSPM signal.

A 30 Hz low-pass filter (4th order Butterworth) was applied to the scale with the maximum en-

ergy to avoid high frequency oscillations unrelated to the arrhythmia that may appear after CWT; all local maxima, defined as points with higher amplitude than both of their immediate neighbors, were then detected. The average of the cycle lengths (CL) was determined from the intervals between the detected peaks and used for the DF calculation ($DF = 1/CL$). Fig. 1A gives a schematic overview of the proposed method. Figs. 1B and C depict the signal morphologies and the respective frequency spectra for a 6 Hz sine wave contaminated with white Gaussian noise with SNR of 1 dB, a 6 Hz sinusoidal wave with presence of the first harmonic (12 Hz) with SNR of 1 dB and a typical AF signal collected at anterior portion of the torso of Patient 1.

$$\psi(t) = -C \cdot \frac{de^{-t^2}}{dt} \tag{1}$$

$$E_{max} = \max_{a} \sum_{n} |W_a(n)^2| \tag{2}$$

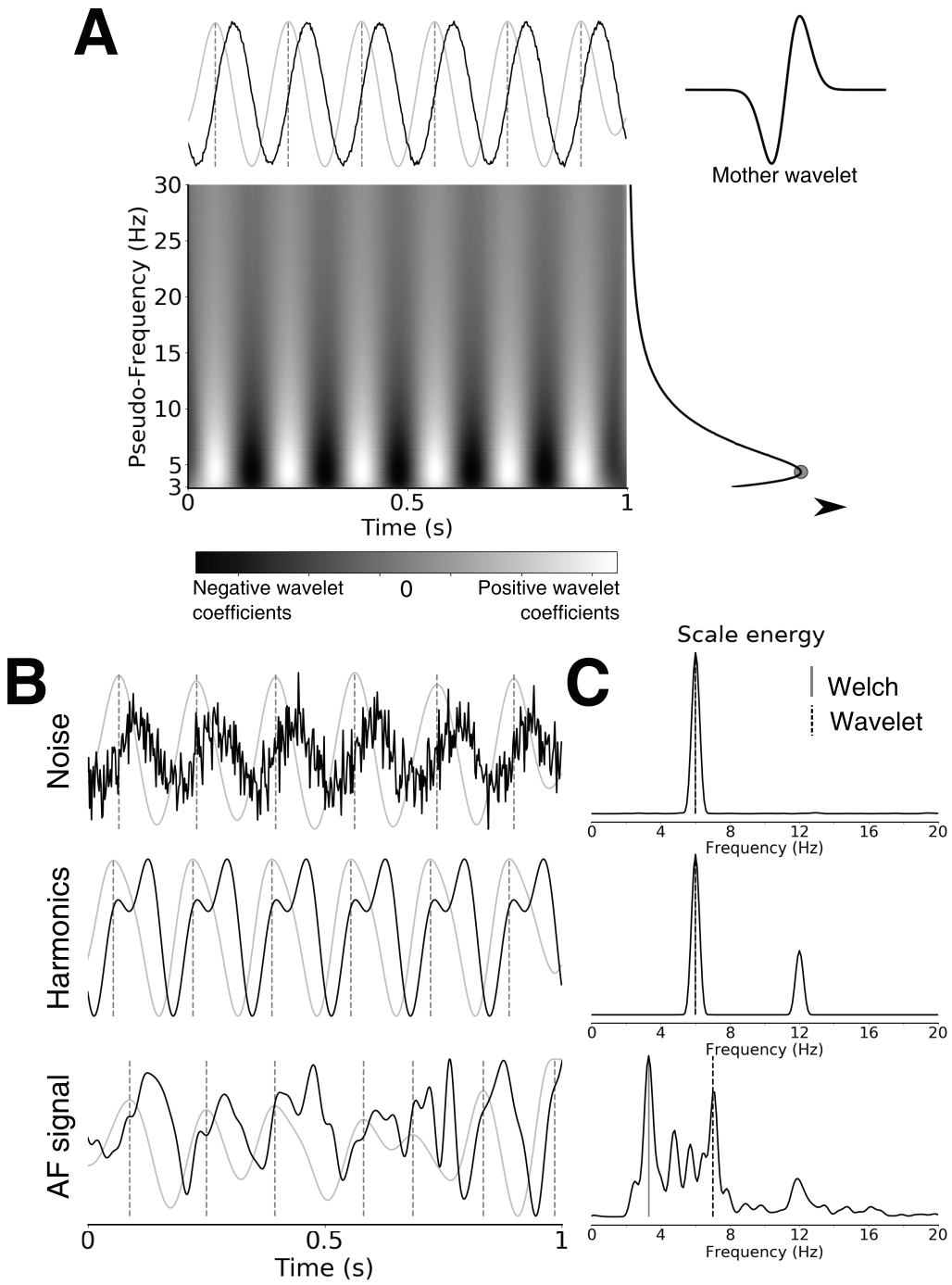

Figure 1: Wavelet method for activation detection and DF estimation. **A:** Schematic of the method. A signal (sine wave with a frequency of 6 Hz, depicted as a black line on the top plot) is used for CWT analysis using a negative first-order Gaussian mother wavelet. The scalogram (bottom) is generated in the pseudo-frequency range of 3 to 30 Hz and the corresponding energy of each scale is calculated. The scale with the maximum energy (top, gray line) is used for the detection of activations, which correspond to the peaks in this scale (top, dashed lines). The average cycle length is used for DF estimation. **B:** Examples of the application of the method in 1-second segments of different signals. Top: 6 Hz sine wave with white Gaussian noise at a SNR of 1 dB. Middle: 6 Hz sinusoidal wave with the presence of a harmonic noise (12 Hz) with SNR of 1 dB. Bottom: signal from the anterior portion of the torso of Patient 1. Black lines represent the original signal, while the gray lines are the CWT at the scale of maximum energy. Dotted lines mark the peaks in the CWT, corresponding to sharp deflections in the original signal. **C:** Corresponding Welch periodograms of the signals in B; the solid line marks the periodogram's highest peak, while the dashed line marks the wavelet estimate. It is possible to see that the method is robust to noise and harmonics in simulated signals, detecting only the inflections related to the signal itself. In the AF signal, only the main repetitive pattern is detected; in this case, the highest peak in the Welch periodogram does not correspond to the DF estimated by the wavelet method.

DFs were estimated by both the proposed method and Welch periodogram. The latter was computed using 2.7 s segments with zero-padding to achieve a frequency step of 0.1 Hz (i.e. $10 \cdot f_S$ samples), Hanning windows and overlap of 90%. Torso DFs were determined by identifying the peak with the highest power in the periodograms withing the AF physiological frequency range (2-15 Hz) [26].

2.5 Driver frequency estimation and spatial distribution

DF maps were generated for both methods by displaying the color coded DF values in the corresponding positions on torso. Atrial HDF values were estimated using the HDF in the BSPM DF maps (HDF_{BSPM}). The accuracy of both methods was assessed by calculating the absolute errors of the HDF_{BSPM} with respect to the atrial HDF; an estimation was considered correct if the absolute error was ≤ 1 Hz. The spatial distribution of the errors between torso DFs and atrial HDFs were analyzed qualitatively based on the location of the driving mechanisms inside the atria (LA or RA). Torso HDF regions, defined as portions of the maps with $|DF - HDF_{BSPM}| \leq 0.5$ Hz, were identified and the percentage of the torso occupied these regions was compared between methods.

DF maps generated with both methods were compared in order to evaluate the effects of the wavelet approach in the DF distributions on the torso. The similarity between the maps was assessed with two-dimensional Pearson's correlation:

$$R = \frac{\sum_m \sum_n (W_{mn} - \mu_W)(M_{mn} - \mu_M)}{\sqrt{\sum_m \sum_n (W_{mn} - \mu_W)^2} \sqrt{\sum_m \sum_n (M_{mn} - \mu_M)^2}} \tag{3}$$

where W and M are DF maps obtained with the wavelet and Welch methods, m and n are matrix indexes and μ represents mean values.

2.6 Robustness of the method to noise and reduction in spatial resolution

The robustness of the atrial HDF estimations by the HDF_{BSPM} of the wavelet method to noise was evaluated under the presence of two different added artifacts: white Gaussian noise and a sinusoidal wave with frequency corresponding to the first harmonic of the atrial HDF (here called harmonic noise). The signal was contaminated with these artifacts with SNRs of 60, 30, 10, 5 and 1

dB and the absolute errors in atrial HDF estimation were used to quantify the effects of the increasing noise. The analyses were expanded to the Welch approach aiming to observe the ability of both methods to estimate the atrial HDF. Additionally, to evaluate the robustness of both methods to lower spatial resolution BSPM lead layouts, the analyses of AF models was reproduced for subsets of the 567 points used for the analyses of computer models (here denominated high-resolution layout - HR) with various numbers of leads: 256 [27], 127[10], 67[9], 64[28], 32 and 16 (Supplementary Fig. 1). For patient data, only the 32 and 16 lead layouts were used for comparison with the original 67 leads layout.

DF maps generated with both the wavelet and Welch methods in all lead layouts were compared with their HR counterpart using two-dimensional Pearson's correlation. Atrial HDF estimations were compared based on the absolute errors between the atrial and torso HDFs. Patterns of spatial distribution were qualitatively compared along lead layouts.

2.7 Statistical analysis

The normality of the data and homogeneity of variances were tested using Anderson-Darling and Bartlett's test, respectively. When the data followed these criteria, paired t-tests were used to compare results from different methods or lead layouts; otherwise, Wilcoxon signed-rank test was used. For comparing results from multiple groups measuring the same parameters (such as with different levels of noise or layouts), Friedman test was used (post-hoc: Nemenyi test); the null-hypothesis of the test is that the measurements with different settings are compatible with each other. Significance for all tests was set at $p < 0.05$.

3 Results

3.1 AF models

3.1.1 Estimation of the atrial HDF

Fig. 2A shows a typical example of a torso DF map calculated by the Welch and the proposed wavelet-based method on a patient with the HDF in the RA. It is of note that DF maps obtained with Welch periodograms present sharper transitions between DF values than in the wavelet method, where the transitions are gradual, resulting in a smoother map. In Fig. 2B we

can observe a signal from a region where a spurious HDF was detected in the Welch method. Although there are several inflections in the signal, only the main repetitive pattern is detected by the wavelet approach. The bottom of Fig. 2B shows how the HDF_{BSPM} obtained by the wavelet method is closer to the atrial HDF, whereas the Welch method detects a higher harmonic peak. Fig. 2C shows an excerpt of an EGM and a BSPM signal from the HDF region in the corresponding map, as marked with a square in Fig. 2A. It is possible to notice that periodicity detected by the wavelet method in the BSPM signal matches the one observed between the activation times in the EGM signal, as marked by the red dots.

Considering all AF simulations, the wavelet method performed better than the Welch approach in approximating the atrial HDF with HDF_{BSPM}, with an relative error ($median$ [IQR]) of 7.14 [3.06 ~ 16.23]% (0.40 [0.20 ~ 1.13] Hz) vs. 60.00 [6.03 ~ 69.36]% (3.30 [0.35 ~ 4.15] Hz), $p = 0.06$ (Fig. 2D). Overall, the wavelet method resulted in correct estimations of atrial HDFs in 81.82% of the simulations, against 45.45% for Welch's estimates (Fig. 2E). DF maps presented low positive correlation between methods ($mean \pm std$: 0.47 ± 0.19, Fig. 2F), indicating important differences in the DF distributions between methods.

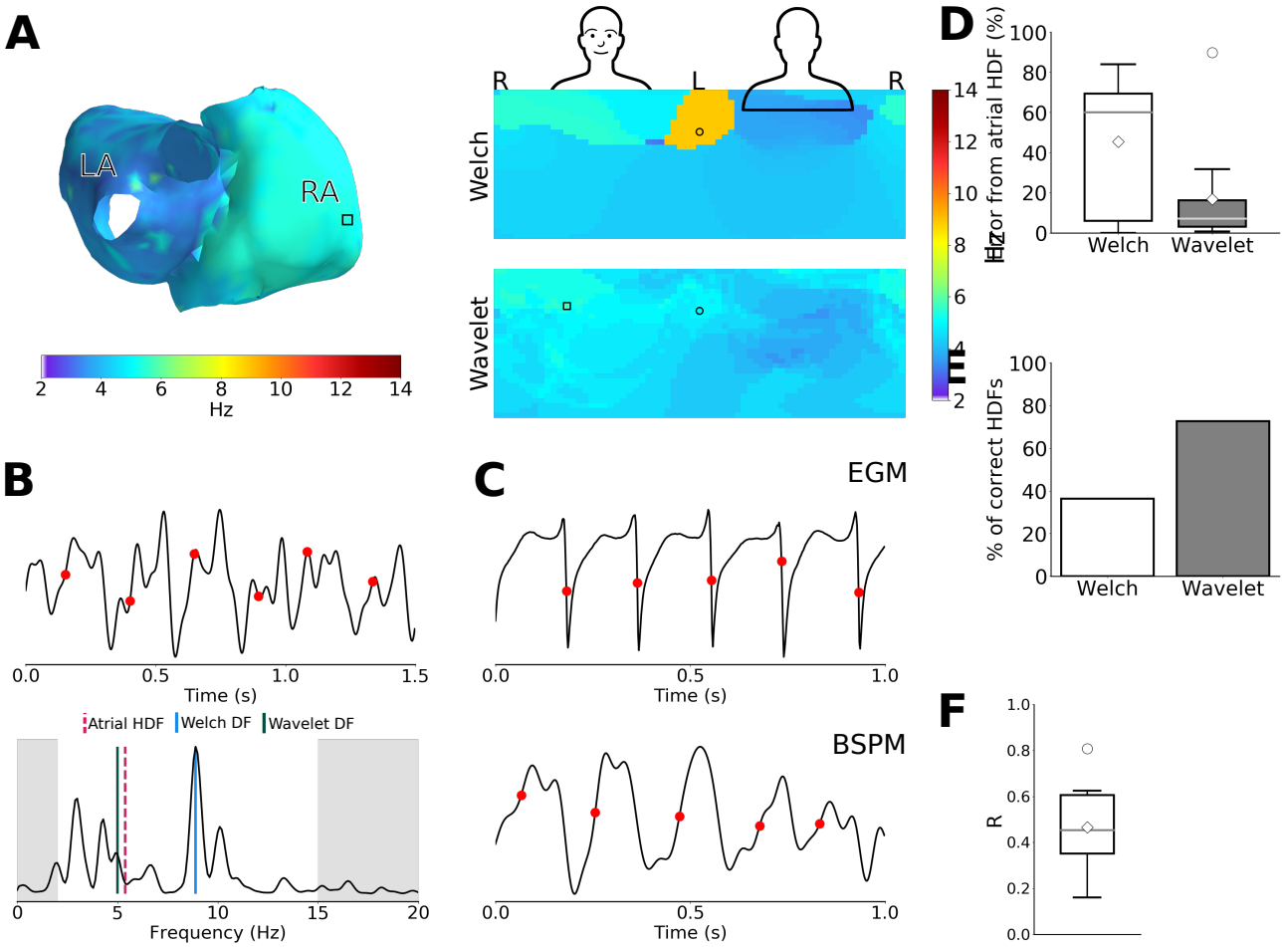

Figure 2: Example of changes in the DF maps with the Welch and wavelet methods from a model with the driver region in the RA. **A:** DF maps of the atria (left) and on the torso (right); torso maps were determined with the Welch (top) and wavelet (bottom) methods (right). It is possible to notice that the wavelet method presents smoother transitions between DFs than those observed in the Welch DF maps. **B:** Segment of the signal at the lead marked with a black circle in A and the respective Welch periodogram. The red dots mark the activations as detected by the wavelet method. Only the main patterns are detected with this method, with the smaller, noisy inflections being ignored. While the DF detected by the Welch method is a harmonic of another frequency in the spectrum, the wavelet method identifies a DF closer to the atrial HDF. **C:** Comparison between a segment of an EGM and a BSPM signal from the HDF regions, marked with a square in A. The periodicity detected by the wavelet method in the BSPM signal matches the number of activations observed in the EGM, as marked in red. **D:** Absolute percentage error in atrial HDF estimation with the HDF_{BSPM} for all simulations. Mean and median values are depicted as diamonds and lines, respectively, while circles are outliers. The wavelet method consistently achieves smaller errors than the Welch approach. **E:** Percentage of simulations with absolute errors from the atrial HDF $\leq$ 1 Hz (i.e. correct estimations of the atrial HDF) for both methods. **F:** 2D correlation coefficient between DF maps obtained with the wavelet and Welch methods for all simulations.

Fig. 3A shows the spatial distribution of absolute errors between atrial and BSPM HDF along the torso for two separate groups depending on which atrium was harboring the rotors and highest DF sites. While similarities were found between methods, the patterns observed present differences in the position of the regions with the smallest errors. For drivers in the LA, the lowest errors were observed on the posterior torso for both methods, mostly on the superior portion for

the Welch method and on the left inferior portion for the wavelet method. For drivers in the RA, errors were smaller on the anterior torso for both methods, especially for wavelet. Fig. 3B indicates that the wavelet method is either better or equivalent to the Welch approach in the majority of the torso, helping highlight the above-mentioned patterns. The percentage of the torso with $|DFs - \text{HDF}_{BSPM}| \leq 0.5Hz$ was statistically equivalent between the Welch and wavelet methods (2.25[1.51 ~ 5.62] vs 5.43[3.49 ~ 5.62] %, respectively, $p = 0.53$)

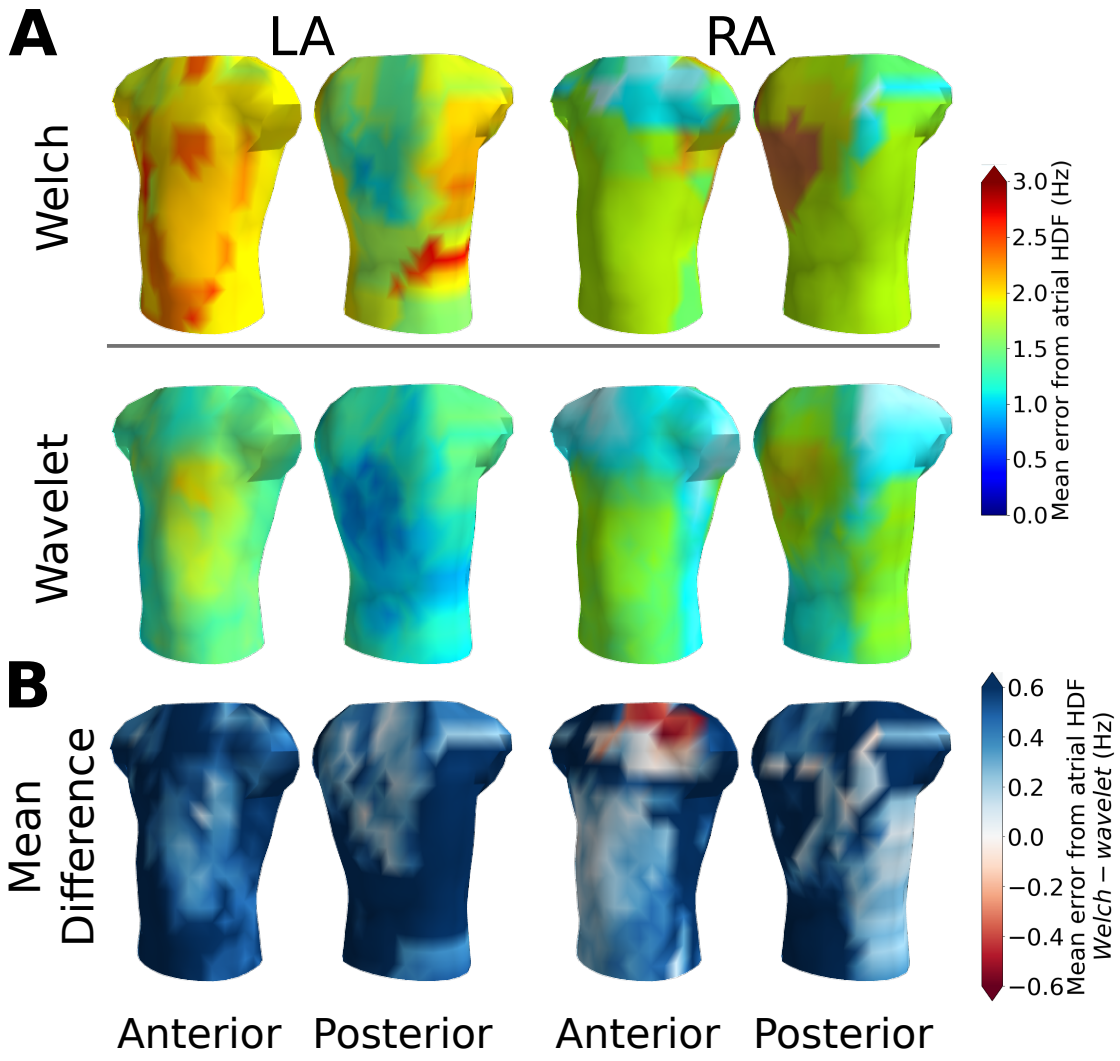

Figure 3: Spatial distribution of absolute errors on the torso for models with respect to the atrial HDF, divided by the atrium where the driver was located. **A:** Absolute differences between torso DFs obtained by both methods and atrial HDF. **B:** Mean difference between the errors from the atrial HDF obtained by both methods. Blue regions indicate portions of the torso where the wavelet performed better (i.e. Welch had higher average errors); in red regions, the Welch method performed better and in white regions, both methods were equivalent. The maps show that the wavelet method achieves lower errors in the majority of the torso. This helps to highlight patterns related to the location of the driving mechanism, such as the predominance of lower errors on the anterior torso for drivers in the RA and on the posterior torso for drivers on the LA.

3.1.2 Effects of noise and reduction in the number of leads

Fig. 4 summarizes the effects of the addition of white Gaussian noise (Fig. 4A), of sinusoidal waves at the harmonics of the atrial HDF (Fig. 4B) and of reducing the number of leads in atrial HDF estimation (Fig. 4C). The wavelet method is robust against Gaussian and harmonic noise, achieving lower mean and median errors than the Welch approach in every scenario. Significant differences in the estimations of the atrial HDF appeared for the wavelet method between the 1 dB and the 30 and 60 dB SNRs for the harmonic noise ($p < 0.01$). For the Welch method, significant differences appeared only with harmonic noise between the 1 dB and the 60 and 30 dB SNRs ($p < 0.05$).

Both Welch and wavelet approaches allow identifying the HDF even when reducing the amount of recorded leads from 567 to 16. Both methods achieve similar results along all lead layouts, with no significant differences ($p = 0.23$ and $p = 0.33$ for Welch and wavelet methods, respectively). Again, the errors obtained with the wavelet method are consistently lower than those obtained with the Welch periodograms. DF maps obtained in layouts with fewer leads correlated better with those from the HR configuration in the wavelet method than in the Welch. The spatial distribution of the differences from the atrial HDF for all lead layouts and both methods is displayed in Supplementary Fig. 2. Global patterns are consistent in both methods for all but the 32 and 16 lead layouts, where major differences appear especially in the simulations from the LA.

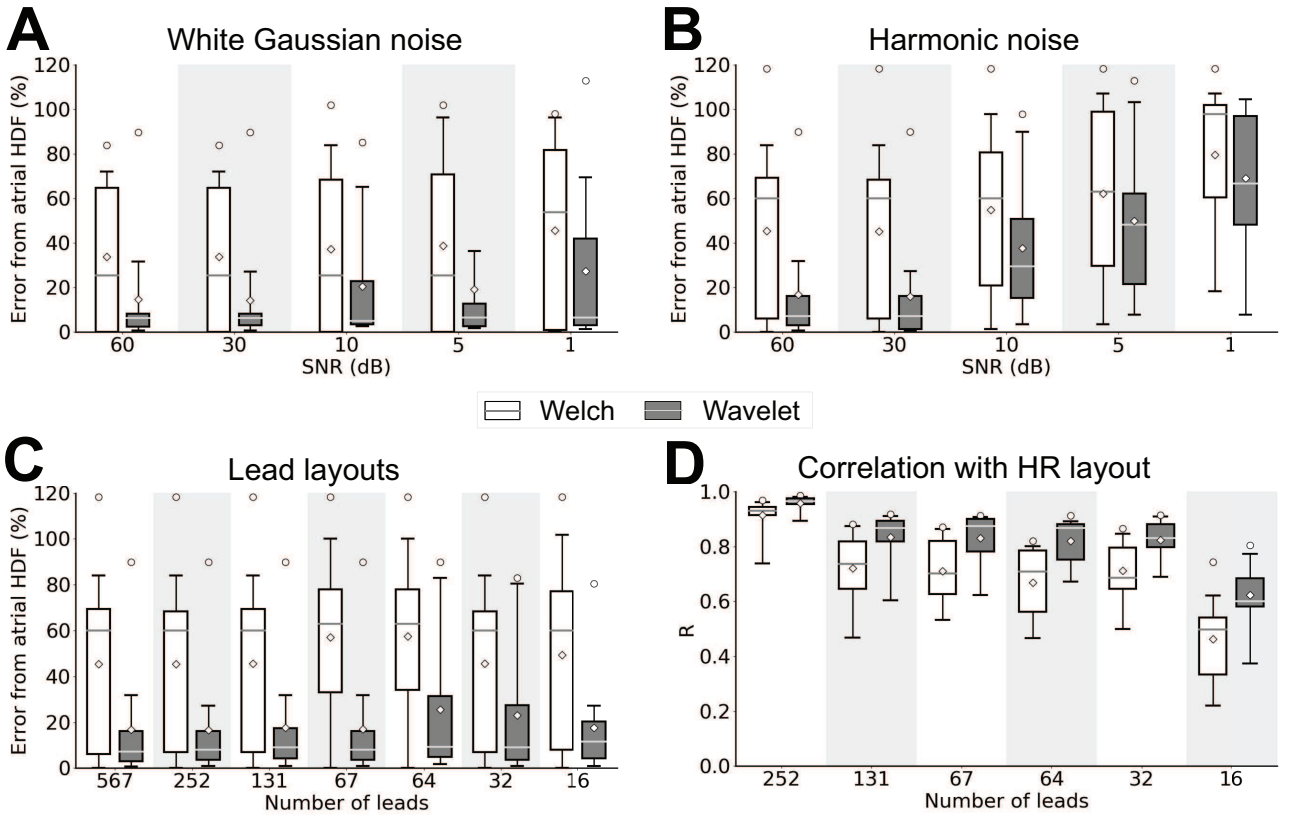

Figure 4: Robustness of the Welch and wavelet methods to uncertainties. **A:** White Gaussian noise with different SNRs. **B:** Harmonic noise with different SNRs. **C:** Reduction in the number of leads. The 2D correlation coefficient between DF maps obtained with the different lead layouts and their HR equivalent is displayed in **D** for all simulations. The wavelet method outperforms the Welch approach in almost every scenario, presenting higher correlation between maps along the lead layouts.

3.2 Patients

3.2.1 Estimation of atrial HDF

Fig. 5A-D gives an example of how the wavelet method can improve the result from Welch analysis in patients. The comparison of DF maps generated by both methods (Fig. 5A) shows a smoother map with the wavelet method, which contains a region of high DFs that do not appear in the Welch map. Looking at segments obtained from the HDF region in the atria (Fig. 5B) and in the BSPM (Fig. 5C), it is possible to observe that the activation times detected by the wavelet method correspond to the most prominent repetitive patterns, detecting cycle lengths similar to those observed in the EGMs. The DF estimates based on the activations is closer to the atrial HDF, while a higher peak in the spectrogram, unrelated to the atrial HDF, increases the error in the Welch method (Fig. 5D).

Analyses were expanded for all AF patients, showing that the atrial HDF estimated in patients

achieved an absolute error of 8.10 [5.50 ~ 13.14]% (0.75 [0.69 ~ 1.06] Hz) for the wavelet method in contrast to the 7.47 [5.59 ~ 19.62]% (0.72 [0.98 ~ 1.98] Hz) obtained by the Welch approach ($p = 0.06$,Fig. 5D). These errors resulted in correct estimations of atrial HDFs in 75.00% of the patients with the wavelet methodology, against 66.67% in the Welch estimates (Fig. 5E). The DF maps obtained with the different methods were more similar than in the models, with a 2D correlation coefficient of 0.63 ± 0.17 (Fig. 5F).

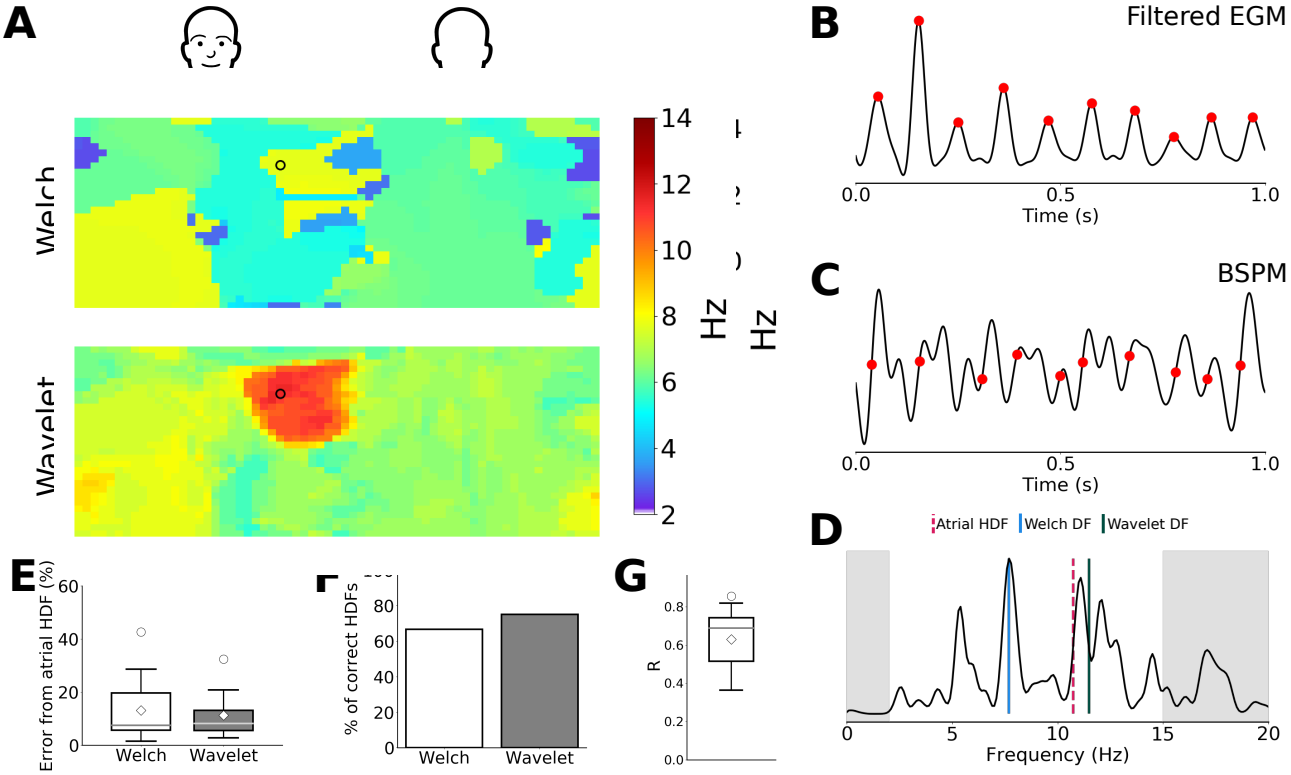

Figure 5: Example of the effect of the wavelet method in comparison to the Welch approach. **A:** DF maps from a patient with atrial HDF of 10.75 Hz in the LA obtained with the Welch (top) and wavelet (bottom) methods. A region with high DFs appears only in the wavelet map. **B:** Filtered EGM signal obtained from the HDF site in the RA **C:** Segment of a signal from the lead marked with a black circle in A. The red dots mark the activation times detected by the wavelet method. It is possible to observe that the periodicity observed in the signals from B and C are similar, indicating good correspondence between the activation times in the EGM and the detections by the wavelet method. **D:** Welch periodogram of the signal in B; peaks in shaded areas are ignored for the DF detection. The DF estimated with the wavelet method is close to the atrial HDF, while a higher peak prevents the detection of the proper DF in the Welch method. **D:** Absolute percentage error in atrial HDF estimation for all patients. Mean and median values are depicted as diamonds and lines, respectively, while circles are outliers. **E:** Percentage of patients with absolute errors from the atrial HDF ≤ 1 Hz (i.e. correct estimations of the atrial HDF) for both methods. **F:** 2D correlation coefficient between DF maps obtained with the wavelet and Welch methods for all patients.

The spatial distribution of the errors from the atrial HDF along the torso is displayed in Fig. 6. In patients with the driver in the LA, distributions were similar along the torso for the Welch method, but revealed lower errors on the anterior portion, especially on the left, for the wavelet approach. For the drivers in the RA, errors were higher on the posterior portion of the torso for

both methods, with the lower errors occurring on the right anterior portion of the torso. The errors with the wavelet method were either equivalent to or lower than those from the Welch approach along all the torso drivers in both atria. The portion of the torso with $|DFs - \text{HDF}_{BSPM}| \leq 0.5Hz$ was significantly different for both methods, occupying $13.41 \pm 7.28\%$ and $3.56 \pm 5.15\%$ of the torso in the Welch and wavelet methods, respectively ($p < 0.01$).

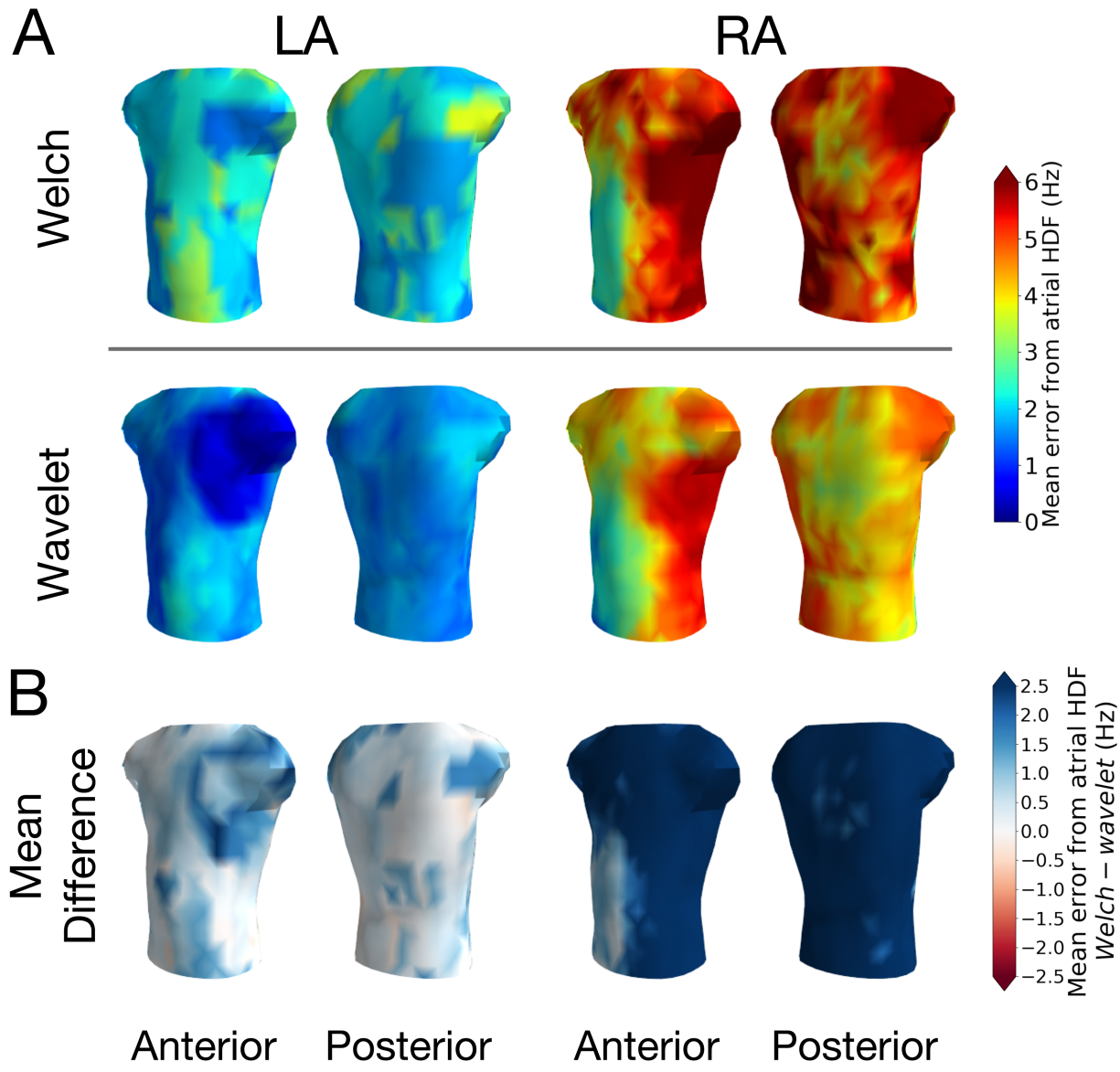

Figure 6: Spatial distribution of absolute errors on the torso for patients with respect to the atrial HDF, divided by the atrium where the driver was located. **A:** Absolute differences between torso DFs obtained by both methods and atrial HDF. **B:** Mean difference between the errors from the atrial HDF obtained by both methods. Blue regions indicate portions of the torso where the wavelet performed better (i.e. Welch had higher average errors); in red regions, the Welch method performed better and in white regions, both methods were equivalent. Errors are either lower or equivalent in the wavelet method when compared with the Welch approach. In the wavelet method, for patients with the driver in the RA, lower errors appear on the anterior portion of the torso, with a clear gradient to the posterior portion. For drivers in the LA, errors are lower on the left portion of the torso.

3.2.2 Effects of reduction in the number of leads

Fig. 7 shows the effect of reducing the number of leads in patient data from 67 leads down to 32 and 16 leads in atrial HDF estimation (Fig. 7A), as well as the correlation between DF maps generated with the reduced layouts in comparison to the original 67 leads (Fig. 7B). There were no significant differences between the atrial HDF estimated with the HDF_{BSPM} for both methods ($p = 0.43$ and $p = 0.79$ for Welch and wavelet, respectively). The spatial distribution in DF maps presented an intermediate positive correlation; when analyzing the spatial distribution of differences from the atrial HDF (Supplementary Fig. 3), the layouts with reduced numbers of leads present similar patterns than the original configuration, but less spatially localized.

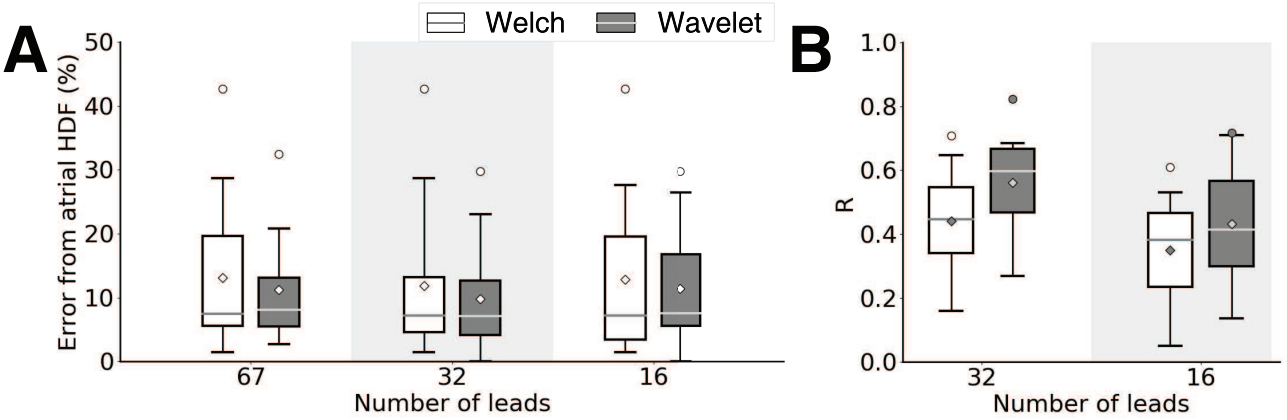

Figure 7: Effects of reducing the number of leads in patient data in outcomes from the Welch and wavelet methods. **A:** Absolute percentage error in atrial HDF estimation. **B:** Correlation between DF maps generated with the original and reduced number of leads

4 Discussion

In this study, a method based on maximum detection in continuous wavelet transform with Gaussian wavelets for the estimation of the DF in BSPM signals has been developed. Since there is no gold standard methodology for non-invasive DF estimation, comparisons were made with the traditional widely applied approach based on peak detection in Welch periodograms. From the results it can be highlighted that the proposed wavelet-based method showed a better accuracy for estimating the arrhythmic mechanism frequency, even under noisy conditions and relative low number of layout leads.

DF analysis has been introduced in the study of the AF dynamics as a means to provide an alternative to the annotation of activations in EGMs, allowing a reliable periodicity measurement of

fibrillatory waves that is more robust to amplitude and morphology changes than manual or automated time analysis [13], [16]. However, frequency analysis is subject to some uncertainties that may significantly alter the resulting DF, such as variation in amplitude, frequency or phase, fractionation, and ventricular influence [13], [16]. Although parallel observation of signals in the time domain may mitigate some of these issues [13], manual correction of the results may be needed to avoid the detection of harmonic DFs and exclusion of noisy leads [9], [10].

Wavelet transform is an intermediary technique between pure time or frequency analyses, providing good localization in both domains [18]. Our methodology incorporates characteristics of both traditional time and frequency analyses into a single approach: the selection of the scale with the highest energy in the AF physiological range acts as a sort of "DF" selection, focusing on the dominant periodic characteristics, but not restricting the analysis to a single frequency component. Using a first-order Gaussian wavelet to perform CWT provides a reliable method for obtaining activation times based on the identification of points with close to singular behavior (i.e. sharp transitions). This avoids the use of derivative-based detection of activations [5], which has an intrinsic high-pass characteristic and might lead to double counting due to the multiple inflections of the AF signal [19].

In this work, comparison with Welch's periodogram method for approximating the atrial HDF indicated that our approach obtains consistently lower errors even in situations with low SNR and with limited lead layouts. Differences in performance between the Wavelet-based method and Welch periodogram are smaller for the patient group compared to modeled AF (75.00% vs 66.67% and 81.82% vs 45.45% respectively). The promising results on mathematical models highlight the usefulness of the proposed technique, although further analyses are required on a larger dataset of patients to validate the statistical significance.

In other studies, the correspondence between surface HDF estimated with Welch periodograms and atrial HDF was stronger than in the results presented here [9], [10]. However, in the mentioned studies, visual inspection of the quality of the signals and/or of the peak detection in the periodograms was conducted, leading to the manual exclusion of problematic leads; this step was not performed in the current study. This allowed for the comparison of both methods in a purely automatic configuration. In this scenario, our results indicate that the wavelet method for DF detection is more suited to unsupervised applications, such as clinical decision support systems.

Correlation between DF maps obtained with the Welch and the wavelet methods suggested the presence of relevant differences in the spatial distribution of DFs. Observation of the DF maps (see Supplementary Figs. 4 and 5) indicates that most of the maps present a global similarity, with regions of similar frequencies appearing in approximately in the same positions even in low correlation cases (e.g. models 2, 3 and 9 and most of the patients). However, the sizes of the regions vary considerably and some HDF_{BSPM} regions appear in different positions, usually due to noisy HDF detections (e.g. models 2, 6 and 11).

Previous studies have evaluated the spatial distribution of DFs and their relationship to the atrial DF patterns [9], [29], [30]. HDFs appearing on the left and posterior portions of the torso correlated better with atrial HDFs inside the LA, whereas HDFs in the RA reflected in BSPM HDFs on the anterior and right portions of the torso [9], [29]. These patterns have been observed here for both methods when analyzing the spatial distribution of errors in atrial HDF estimation; however, the wavelet method presented in average smaller absolute errors in most of the torso. This resulted in clearer error gradients for this method, helping highlight the predominance of lower errors on the anterior torso for drivers in the RA vs. on the posterior torso for drivers in the LA. Further studies with spatially detailed invasive measurements are needed to validate whether the locations of the HDF_{BSPM} in the wavelet method increase the ability of the BSPM to approximate atrial DF distributions.

In addition to the above-mentioned improvements in DF analysis for AF, the proposed methodology also has the potential to aid studies in the time and phase domains. The propagation of activation wavefronts can be used for the non-invasive study of AF patterns [5] and is addressed by our methodology, which relies on activation times for DF estimation. Although the precise marking of AF wavefronts can be a difficult task in BSPM due to the multiple inflections of the fibrillatory waves, the method proposed here delivers consistent estimations of these points, that could be used to improve other time-based analysis such as those presented in [5] and [6].

In phase analysis, precise and/or time-specific detection of DFs is essential for conditioning signals before applying the Hilbert transform, be that by narrow band-pass filtering around the DF to stabilize the rotational activity [7] or for detrending the signals to achieve more consistent results [19]. Since our methodology identifies individual waves in the BSPM signals and estimates each CL, instantaneous DF estimation is possible and can be used in more sophisticated phase

analysis algorithms. Additionally, the errors in DF estimation with respect to the atrial HDF were smaller, which guarantees that the narrow band-pass filtering is focusing the analyses in the frequencies truly related to the rotors.

5 Study limitations

In this study, a limited number of 11 simulations and 12 patients with AF were used to validate the methodology. This number may not account for the complexity and variability of AF in the general population and the methodology should be further validated in larger data sets. The AF models were contaminated with white Gaussian noise, but it might not represent all forms of noise collected during clinical studies with non-invasive cardiac recordings. Although the Welch approach has been a widely applied method for estimating DF from BSPM maps, and that the present study proposed a method that does perform better, it should be emphasized that currently there is no gold standard method for estimating DF from BSPM maps.

Patient data were recorded under adenosine infusion, which speeds-up the atrial activation frequency in a way that might not be present in basal AF, resulting in higher atrial HDFs. This paper does not address the effects on DF estimation after ventricular far-field cancellation on the AF body surface signals.

6 Conclusion

Estimations of atrial HDFs using BSPM can be improved by the use of the continuous wavelet transform based algorithm presented in this work. More precise estimations can enhance the diagnostic ability of the DF analyses in BSPM and may improve the outcomes of time or phase analyses, increasing the value of the BSPM as a low complexity tool for early diagnosis and follow-up.

7 Acknowledgments

This study was supported in part by grants from São Paulo Research Foundation (2017/19775-3), Instituto de Salud Carlos III FEDER (Fondo Europeo de Desarrollo Regional PI17/01106) and Generalitat Valenciana Grants (AICO/2018/267).

Disclosures: M. S. Guillem is shareholder of Corify Care S.L.

References

[1] P. Kirchhof, S. Benussi, D. Kotecha, A. Ahlsson, D. Atar, B. Casadei, M. Castella, H.-C. Diener, H. Heidbuchel, J. Hendriks, *et al.*, "2016 esc guidelines for the management of atrial fibrillation developed in collaboration with eacts", *European journal of cardio-thoracic surgery*, vol. 50, no. 5, e1–e88, 2016.

[2] F. Atienza, J. Almendral, J. M. Ormaetxe, Á. Moya, J. D. Martínez-Alday, A. Hernández-Madrid, E. Castellanos, F. Arribas, M. Á. Arias, L. Tercedor, *et al.*, "Comparison of radiofrequency catheter ablation of drivers and circumferential pulmonary vein isolation in atrial fibrillation: A noninferiority randomized multicenter radar-af trial", *Journal of the American College of Cardiology*, vol. 64, no. 23, pp. 2455–2467, 2014.

[3] S. M. Narayan, D. E. Krummen, K. Shivkumar, P. Clopton, W.-J. Rappel, and J. M. Miller, "Treatment of atrial fibrillation by the ablation of localized sources: CONFIRM (conventional ablation for atrial fibrillation with or without focal impulse and rotor modulation) trial", *Journal of the American College of Cardiology*, vol. 60, no. 7, pp. 628–636, 2012.

[4] M. S. Guillem, A. M. Climent, M. Rodrigo, F. Fernández-Avilés, F. Atienza, and O. Berenfeld, "Presence and stability of rotors in atrial fibrillation: Evidence and therapeutic implications", *Cardiovascular research*, vol. 109, no. 4, pp. 480–492, 2016.

[5] M. S. Guillem, A. M. Climent, F. Castells, D. Husser, J. Millet, A. Arya, C. Piorkowski, and A. Bollmann, "Noninvasive mapping of human atrial fibrillation", *Journal of cardiovascular electrophysiology*, vol. 20, no. 5, pp. 507–513, 2009.

[6] E. A. P. Alday, M. A. Colman, P. Langley, and H. Zhang, "Novel non-invasive algorithm to identify the origins of re-entry and ectopic foci in the atria from 64-lead ecgs: A computational study", *PLoS computational biology*, vol. 13, no. 3, e1005270, 2017.

[7] M. Rodrigo, M. S. Guillem, A. M. Climent, J. Pedrón-Torrecilla, A. Liberos, J. Millet, F. Fernández-Avilés, F. Atienza, and O. Berenfeld, "Body surface localization of left and right atrial high-frequency rotors in atrial fibrillation patients: A clinical-computational study", *Heart Rhythm*, vol. 11, no. 9, pp. 1584–1591, 2014.

[8] C. Ramanathan, R. N. Ghanem, P. Jia, K. Ryu, and Y. Rudy, "Noninvasive electrocardiographic imaging for cardiac electrophysiology and arrhythmia", *Nature medicine*, vol. 10, no. 4, p. 422, 2004.

[9] M. S. Guillem, A. M. Climent, J. Millet, Á. Arenal, F. Fernández-Avilés, J. Jalife, F. Atienza, and O. Berenfeld, "Noninvasive localization of maximal frequency sites of atrial fibrillation by body surface potential mapping", *Circulation: Arrhythmia and Electrophysiology*, vol. 6, no. 2, pp. 294–301, 2013.

[10] F. J. Vanheusden, G. S. Chu, X. Li, J. Salinet, T. P. Almeida, N. Dastagir, P. J. Stafford, G. A. Ng, and F. S. Schlindwein, "Systematic differences of non-invasive dominant frequency estimation compared to invasive dominant frequency estimation in atrial fibrillation", *Computers in biology and medicine*, vol. 104, pp. 299–309, 2019.

[11] J. Jalife, O. Berenfeld, and M. Mansour, "Mother rotors and fibrillatory conduction: A mechanism of atrial fibrillation", *Cardiovascular research*, vol. 54, no. 2, pp. 204–216, 2002.

[12] P. Sanders, O. Berenfeld, M. Hocini, P. Jais, R. Vaidyanathan, L.-F. Hsu, S. Garrigue, Y. Takahashi, M. Rotter, F. Sacher, *et al.*, "Spectral analysis identifies sites of high-frequency activity maintaining atrial fibrillation in humans", *Circulation*, vol. 112, no. 6, pp. 789–797, 2005.

[13] J. Ng and J. J. Goldberger, "Understanding and interpreting dominant frequency analysis of af electrograms", *Journal of cardiovascular electrophysiology*, vol. 18, no. 6, pp. 680–685, 2007.

[14] F. Atienza, J. Almendral, J. Jalife, S. Zlochiver, R. Ploutz-Snyder, E. G. Torrecilla, A. Arenal, J. Kalifa, F. Fernández-Avilés, and O. Berenfeld, "Real-time dominant frequency mapping and ablation of dominant frequency sites in atrial fibrillation with left-to-right frequency gradients predicts long-term maintenance of sinus rhythm", *Heart Rhythm*, vol. 6, no. 1, pp. 33–40, 2009.

[15] X. Li, J. L. Salinet, T. P. Almeida, F. J. Vanheusden, G. S. Chu, G. A. Ng, and F. S. Schlindwein, "An interactive platform to guide catheter ablation in human persistent atrial fibrillation using dominant frequency, organization and phase mapping", *Computer methods and programs in biomedicine*, vol. 141, pp. 83–92, 2017.

[16] J. Ng, A. H. Kadish, and J. J. Goldberger, "Effect of electrogram characteristics on the relationship of dominant frequency to atrial activation rate in atrial fibrillation", *Heart Rhythm*, vol. 3, no. 11, pp. 1295–1305, 2006.

[17] I. Romero, E. Fleck, and C. Kriatselis, "Frequency analysis of atrial fibrillation surface and intracardiac electrograms during pulmonary vein isolation", *Europace*, vol. 13, no. 9, pp. 1340–1345, 2011.

[18] S. Mallat and W. L. Hwang, "Singularity detection and processing with wavelets", *IEEE transactions on information theory*, vol. 38, no. 2, pp. 617–643, 1992.

[19] R. Vijayakumar, S. K. Vasireddi, P. S. Cuculich, M. N. Faddis, and Y. Rudy, "Methodology considerations in phase mapping of human cardiac arrhythmias", *Circulation: Arrhythmia and Electrophysiology*, vol. 9, no. 11, e004409, 2016.

[20] M. W. Krueger, G. Seemann, K. Rhode, D. U. Keller, C. Schilling, A. Arujuna, J. Gill, M. D. O'Neill, R. Razavi, and O. Dossel, "Personalization of atrial anatomy and electrophysiology as a basis for clinical modeling of radio-frequency ablation of atrial fibrillation", *IEEE transactions on medical imaging*, vol. 32, no. 1, pp. 73–84, 2012.

[21] M. Rodrigo, A. M. Climent, A. Liberos, F. Fernández-Avilés, O. Berenfeld, F. Atienza, and M. S. Guillem, "Highest dominant frequency and rotor positions are robust markers of driver location during noninvasive mapping of atrial fibrillation: A computational study", *Heart rhythm*, vol. 14, no. 8, pp. 1224–1233, 2017.

[22] J. T. Koivumäki, G. Seemann, M. M. Maleckar, and P. Tavi, "In silico screening of the key cellular remodeling targets in chronic atrial fibrillation", *PLoS computational biology*, vol. 10, no. 5, e1003620, 2014.

[23] V. M. Garca-Molla, A. Liberos, A. Vidal, M. Guillem, J. Millet, A. Gonzalez, F.-J. Martnez-Zaldvar, and A. M. Climent, "Adaptive step ode algorithms for the 3d simulation of electric heart activity with graphics processing units", *Computers in biology and medicine*, vol. 44, pp. 15–26, 2014.

[24] M. Rodrigo, A. M. Climent, A. Liberos, F. Fernández-Avilés, O. Berenfeld, F. Atienza, and M. S. Guillem, "Technical considerations on phase mapping for identification of atrial reentrant

activity in direct-and inverse-computed electrograms", *Circulation: Arrhythmia and Electrophysiology*, vol. 10, no. 9, e005008, 2017.

[25] M. Guillem, A. Quesada, V. Donis, A. Climent, N. Mihi, J. Millet, and F. Castells, "Surface wavefront propagation maps: Non-invasive characterization of atrial flutter circuit", *Int J Bioelectromagn*, vol. 11, pp. 22–26, 2009.

[26] J. L. Salinet, J. H. Tuan, A. J. Sandilands, P. J. Stafford, F. S. Schlindwein, and G. A. Ng, "Distinctive patterns of dominant frequency trajectory behavior in drug-refractory persistent atrial fibrillation: Preliminary characterization of spatiotemporal instability", *Journal of cardiovascular electrophysiology*, vol. 25, no. 4, pp. 371–379, 2014.

[27] M. Haïssaguerre, M. Hocini, A. Denis, A. J. Shah, Y. Komatsu, S. Yamashita, M. Daly, S. Amraoui, S. Zellerhoff, M.-Q. Picat, *et al.*, "Driver domains in persistent atrial fibrillation", *Circulation*, vol. 130, no. 7, pp. 530–538, 2014.

[28] J. L. Salinet, V. G. Marques, M. Mazzetto, E. D. Camargo, C. A. Pastore, and I. A. Cestari, "A 64-lead body surface potential mapping system", in *2017 Computing in Cardiology (CinC)*, IEEE, 2017, pp. 1–4.

[29] M. Bojarnejad, J. R. Blake, J. Bourke, E. Shepherd, A. Murray, and P. Langley, "Non-invasive estimation of left atrial dominant frequency in atrial fibrillation from different electrode sites: Insight from body surface potential mapping", *Journal of atrial fibrillation*, vol. 7, no. 3, 2014.

[30] M. Rodrigo, A. Climent, A. Liberos, F. Fernández-Aviles, F. Atienza, M. Guillem, and O. Berenfeld, "Minimal configuration of body surface potential mapping for discrimination of left versus right dominant frequencies during atrial fibrillation", *Pacing and Clinical Electrophysiology*, vol. 40, no. 8, pp. 940–946, 2017.